REPUBLIQUE ALGERIENNE DEMOCRATIQUE ET POPULAIRE
MINISTERE DE L'ENSEIGNEMENT SUPERIEUR ET DE LA RECHERCHE SCIENTIFIQUE
UNIVERSITE MOHAMED BOUDIAF - M'SILA

FACULTE DES SCIENCES
DEPARTEMENT PHYSIQUE
N° : Ph/ENR/04/2024

DOMAINE : Sciences de la matière
FILIERE : Physique
OPTION : Physique Énergétique et Energies renouvelables

Mémoire présenté pour l'obtention
Du diplôme de Master Académique

Par: Assaous Ayoub Abdelyakine

Intitulé

Numerical Modelling of a Diffuser Effect on the Airflow Structure within a solar chimney

Soutenu le 17 / 09 /2024 devant le jury composé de:

Dr Kalli Sihem	Université Mohamed Boudiaf- M'sila	Présidente
Dr Boulechfar Hichem	Université Mohamed Boudiaf- M'sila	Rapporteur
Dr Tahrour Farouk	Université Mohamed Boudiaf- M'sila	Examinateur

Année universitaire : 2023/2024

Dedications

This work is dedicated to my parents who stayed with me to get to this point in my life

And to my brothers and sisters and family who encouraged me to complete my studding career

Acknowledgments

I would like to extend my deepest gratitude to my supervisor, **Dr Boulechfar Hichem**, for his invaluable patience and insightful feedback.

My sincere gratitude to **Dr. Kalli Sihem** for presiding my master's defense jury and my sincere thanks to **Dr. Tahrour Farouk** for examining my Master thesis manuscript.

Table of contents

Chapter III: Numerical Simulation Software

CHAPTER IV: Results and Discussion

Nomenclature

Latin letters:

T_h	Hot temperature	[K]
T_c	Cold temperature	[K]
h_d	Diffuser's height	[m]
h_c	Collector's height	[m]
P	Pressure	[Pa]
r, z	Cylindrical coordinate	[m]
D_c	Collector diameter	[m]
t	Time	[s]
g	Gravitational acceleration	[m/s^2]
Cp	Specific heat capacity	[$J.kg^{-1}.\ k^{-1}$]
v	Velocity	[m/s]
Pr	Prandtl number, $= \frac{v}{\alpha}$	
Ra	Rayleigh number, $= \frac{g\,\beta\,\Delta T\,D^3}{\upsilon\,\alpha}$	
v_r	Velocity component in (r) direction	[m/s]
v_z	Velocity component in (z) direction	[m/s]
v_θ	Velocity component in (θ) direction	[m/s]
r^+	Dimensionless radial coordinates	
z^+	Dimensionless z coordinates	
T^+	Dimensionless temperature	
P^+	Dimensionless pressure	
${v_r}^+$	Dimensionless velocity component	
${v_z}^+$	Dimensionless velocity component	
${v_\theta}^+$	Dimensionless velocity component	

Greek letters:

β_T	Coefficient of thermal expansion	[1/K]
ρ	Density of the fluid	[kg/m^3]
λ	Thermal conductivity	[w/m. k]
α	Thermal diffusivity	[m^2 /s]
μ	Dynamic viscosity	[kg. m^{-1} .s^{-1}]
y	Kinematic viscosity	[m^2/s]
θ	Cylindrical coordinate	[rad]

Subscripts:

r, θ, z	Cylindrical coordinate

Superscripts:

+	Dimensionless

List of figures

Chapter I

Chapter II

Chapter III

Chapter IV

Introduction

The global energy consumption rates are escalating due to the prevalent use of traditional energy sources such as coal, petroleum, and gas. These conventional energies are often credited as the main catalysts for the swift economic expansion in the twenty-first century. However, this increased reliance on such energy sources also brings with it heightened health and environmental hazards, as well as a surge in greenhouse gas emissions.

Solar chimney technology, which harnesses solar power, operates on the principle of free convection caused by a fluid density gradient change. This gradient is created by the temperature difference between the ground and the collector within the system. As a result, an airflow is generated within the enclosure, which ascends to drive the turbines responsible for electricity production.

Our computational analysis is centered on examining the influence of a diffuser height on the performance of the solar chimney by altering the development of the airflow within the system.

The structure of the manuscript is outlined as follows:

The first chapter, titled “Introduction to solar chimney technology,” provides a comprehensive overview of solar chimney system; It gradually delves into the specifics of solar chimney technology. The chapter concludes with a literature review and a discussion of previous studies related to the topic.

The second chapter, titled “Mathematical model formulation,” begins by presenting the problem of an axisymmetric solar chimney. This is depicted through a schematic figure to provide a clearer and more detailed understanding of the geometry.

Next, we delve into the description of the problem, employing governing equations in cylindrical coordinates and utilizing the Boussinesq approximation. We also consider appropriate assumptions and mathematical formalisms to simplify the case under study.

The third chapter delves into the numerical simulation software. It provides a brief overview of the Comsol Multiphysics software and outlines the numerical simulation procedures used to

solve the fundamental equations of the problem. It also includes a straightforward definition of the finite element method, which serves as the foundational meshing method of the software.

In the final chapter, we present various results, accompanied by detailed interpretations and discussions.

The chapter concludes with a summary that emphasizes the key findings.

Chapter I

Introduction to solar chimney technology

1.Introduction

The quantity of energy consumption has significantly increased with the advancement of technology and industrialization of countries. Increasing the capacity of power grids depends on the investment and production of new power plant units

There is a growth trend in the implementation of renewable energy sources in the whole world today. There are also significant investments into research and development of new concepts that are related to the production of electricity and also thermal energy. New concepts that produce electricity through the utilization of natural resources (solar and wind energy) are of special interest

Solar chimney technology, also known as solar updraft tower or the Solar Chimney Power Plant (SCPP) is a renewable energy method that harnesses the sun's thermal energy to generate electricity. It relies on the natural principle of convection, where hot air rises and cool air sinks. The solar chimney consists of a tall vertical tower, a collector, and a turbine system

1. Solar chimney key component

2.1 Solar collector:

The solar collector is usually a large, transparent, greenhouse-like structure surrounding the base of the tower. This structure allows sunlight to pass through and heat the air inside. The ground within the collector is covered with a dark, heat-absorbing material to enhance the heating process.

Figure 1: Solar collector **[1]**

1.2 Tower:

The tower is a tall, vertical structure located at the center of the solar collector is designed to create a temperature difference between the air inside the collector and the outside atmosphere. The tower is typically made of lightweight and heat-absorbing materials.

Figure 2: Solar tower **[2]**

1.3 Turbine system:

At the base of the tower, there is a turbine system connected to a generator. The low-pressure zone at the tower's base draws air from the surroundings into the collector The incoming air is accelerated as it passes through the turbine, driving the generator and producing electricity.

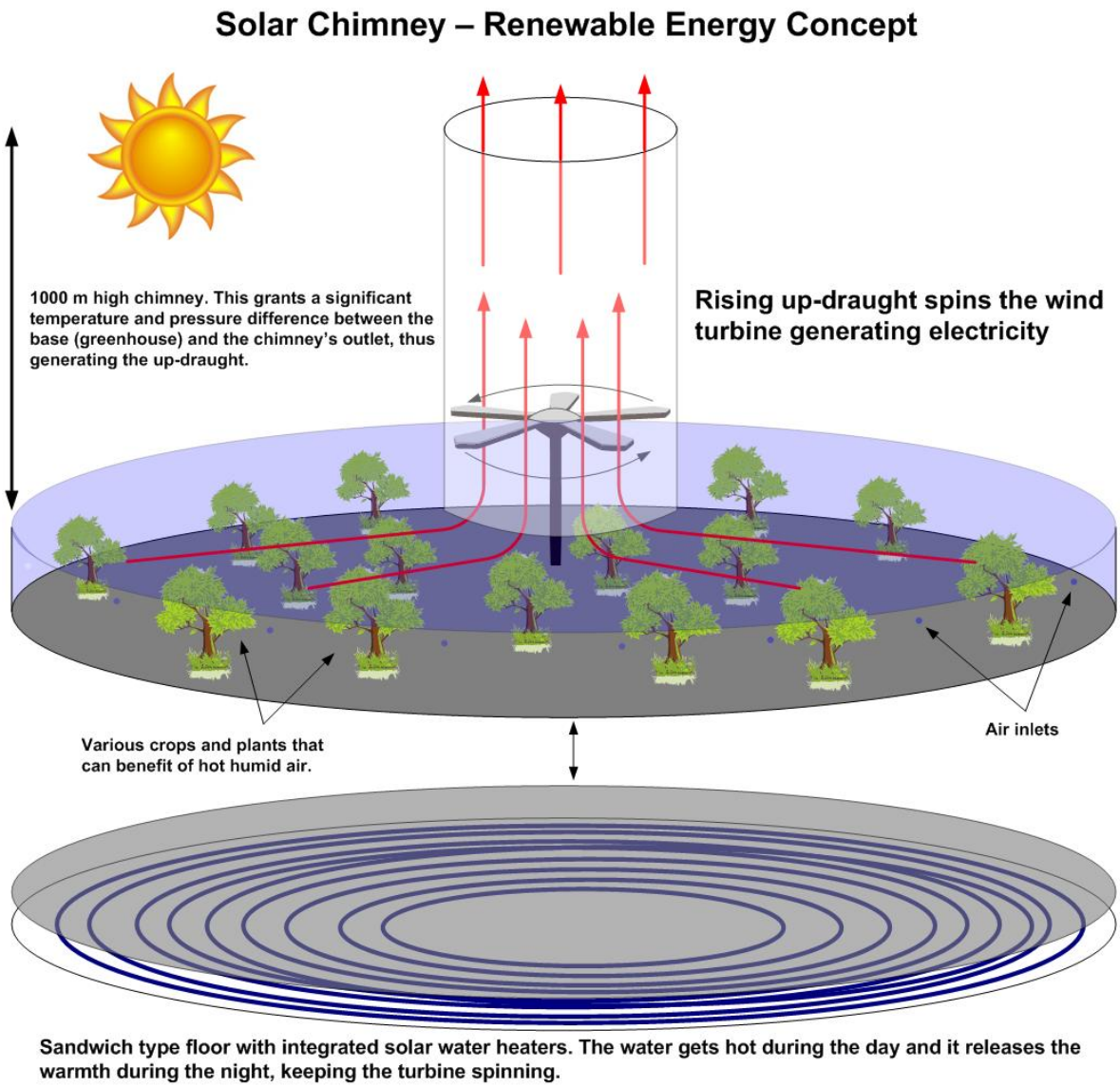

Figure 3: Turbine system **[3]**

1.4 Diffuser

A diffuser, in a general sense, is a device that spreads or scatters a substance. In fluid dynamics, a diffuser is a device that slows down the fluid flow and increases its static pressure. This can be achieved through various designs, such as a diverging duct or a series of vanes.

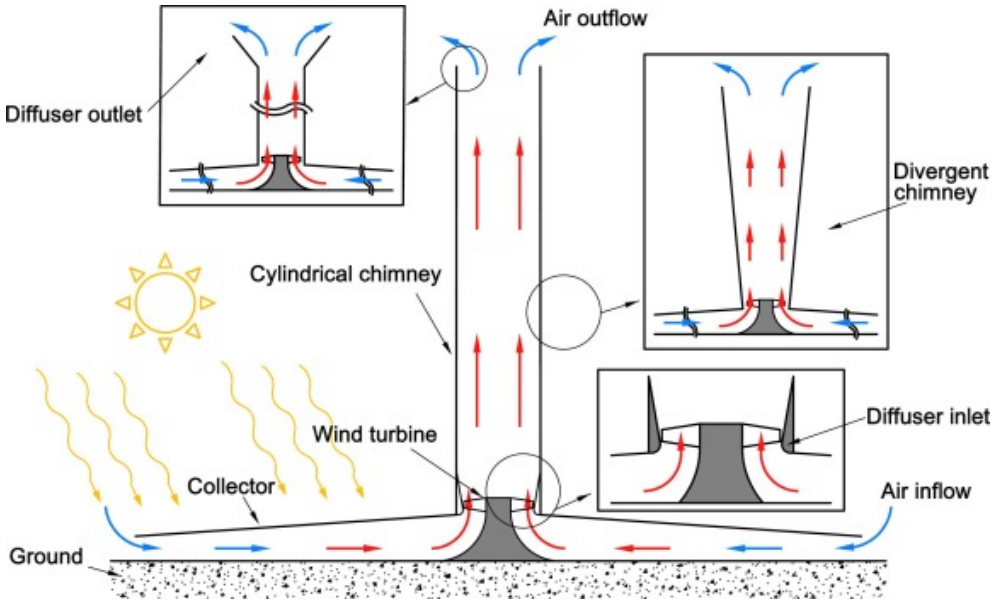

Figure 4: Diffuser diagram **[4]**

2. Solar chimney applications

3.1 Power generation:

The primary application of solar chimneys is large-scale electricity generation. Solar chimneys can be used to produce electricity to power residential areas, industrial facilities, or even contribute to the grid.

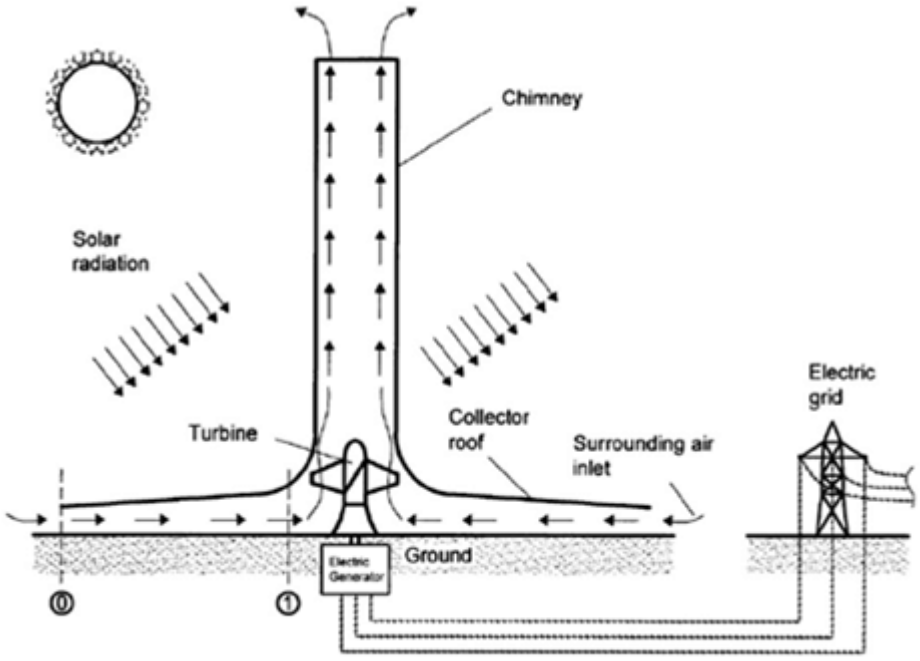

Figure 5: Power generation **[5]**

3.2 Desalination:

Solar chimneys can be integrated into desalination plants. The generated electricity can be used to power the desalination process, providing a sustainable solution to address water scarcity issues in arid regions.

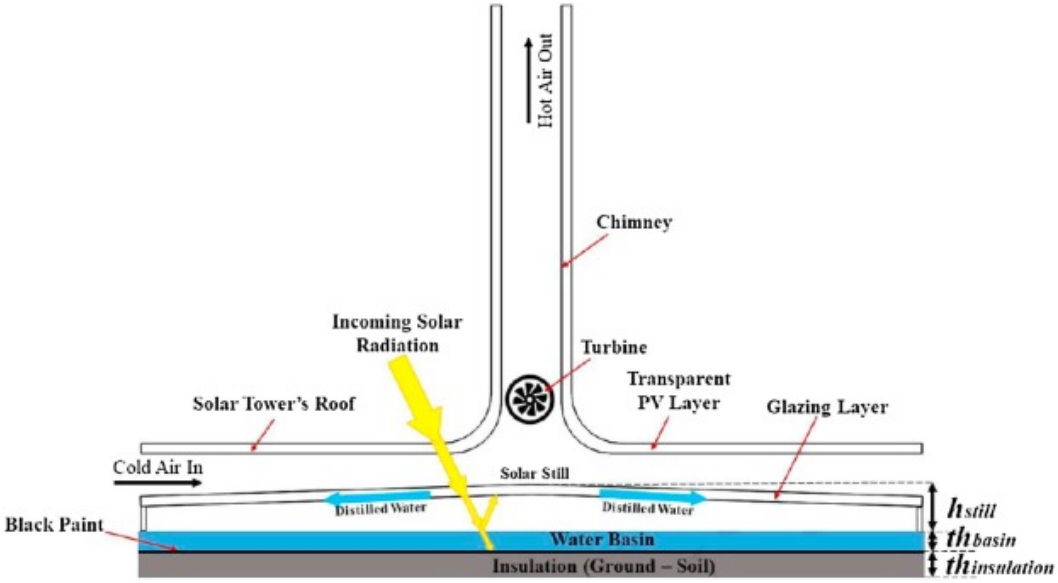

Figure 6: Desalination prototype **[6]**

3.3 Space heating and cooling:

Solar chimneys can be adapted for space heating in buildings during cold seasons. Conversely, the system can be reversed to provide cooling by channeling air through the collector during hot periods.

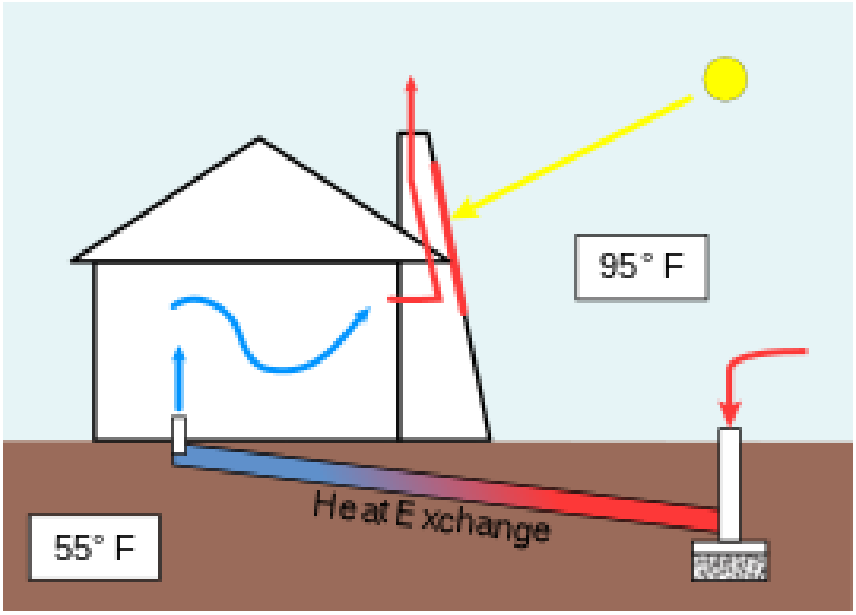

Figure 7: Passive home cooling and heating **[7]**

3.4 Drying process:

Solar chimneys can be used for drying agricultural products and food processing. The hot air generated within the collector can be directed into drying chambers, contributing to the preservation and processing of crops.

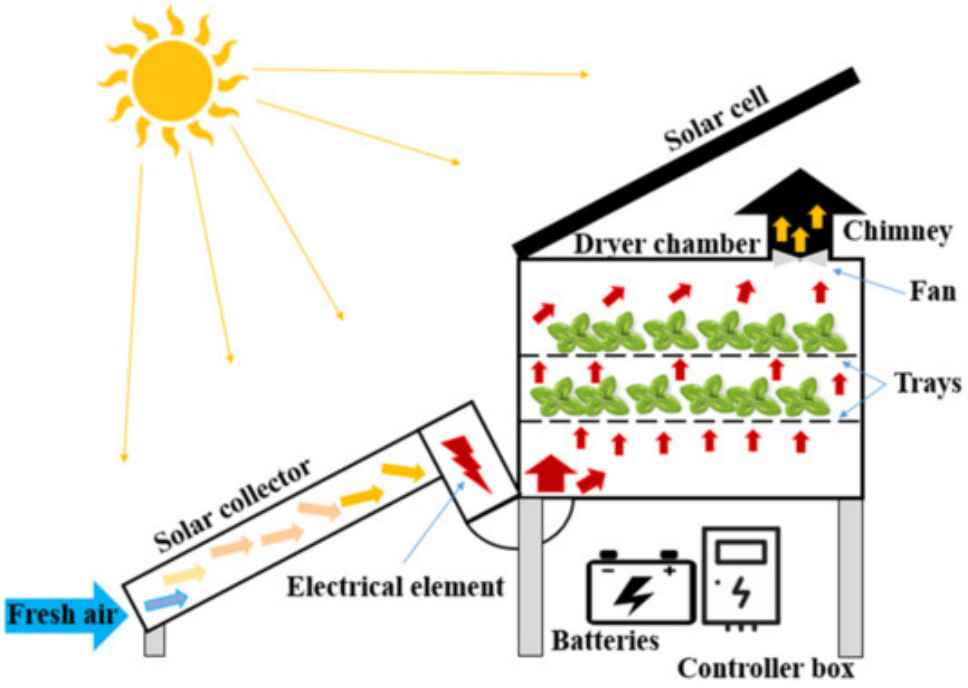

Figure 8: Food drying method **[8]**

3.5 Agricultural and environmental applications:

Solar chimneys can play a role in mitigating environmental issues. For example, they can be used to enhance air circulation in certain agricultural areas, preventing the formation of frost during cold nights.

Figure 9: Greenhouse effect **[9]**

3.6 Remote power generation:

In remote or off-grid areas, solar chimneys can provide a reliable source of electricity without the need for extensive infrastructure. This can be particularly valuable in regions with abundant sunlight and limited access to conventional power sources.

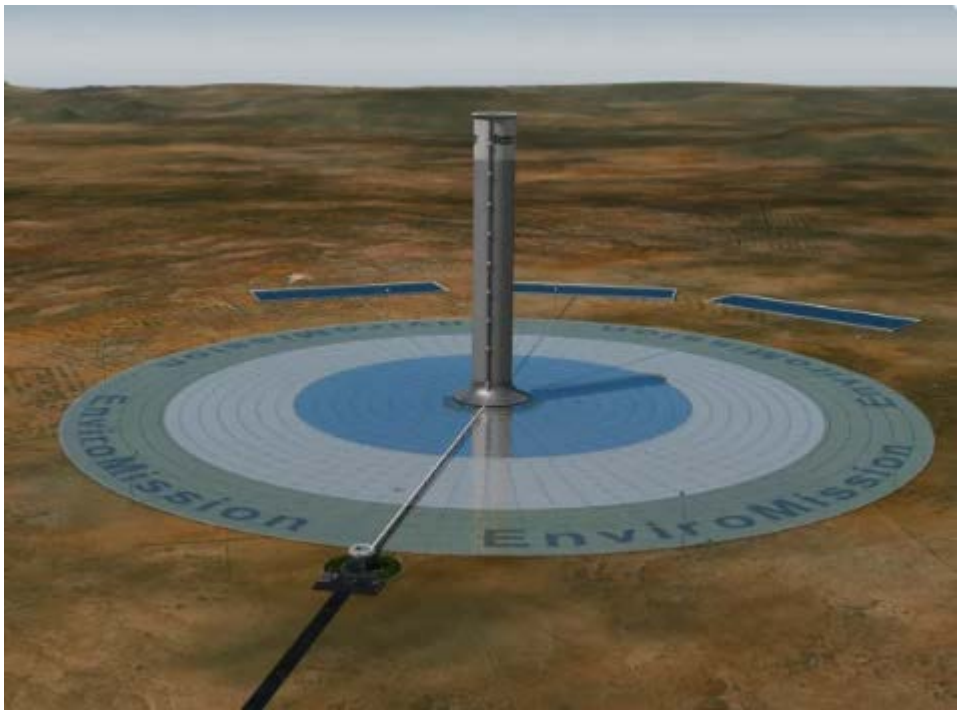

Figure 10: numerical modeling of solar chimney **[10]**

3.7 Research and education:

Solar chimneys can serve as educational tools for studying thermodynamics, fluid dynamics, and renewable energy concepts. Constructing smaller-scale models can be a practical way to demonstrate these principles in educational settings.

Figure 11: Manzanares SCPP **[11]**

3.8 Hybrid systems:

Solar chimney technology can be integrated with other renewable energy systems, such as solar photovoltaic or wind turbines, to create hybrid power plants. This approach can enhance energy production by leveraging multiple renewable sources.

Figure 12: SCPP in Europe **[12]**

3. Working principals

The sun's natural heat warms the air in the chimney, causing it to rise and create a draft that moves the hot air out of the structure. This heating process causes the cooler air from below to be pulled into the chimney for heating while the hot air is released from the top.

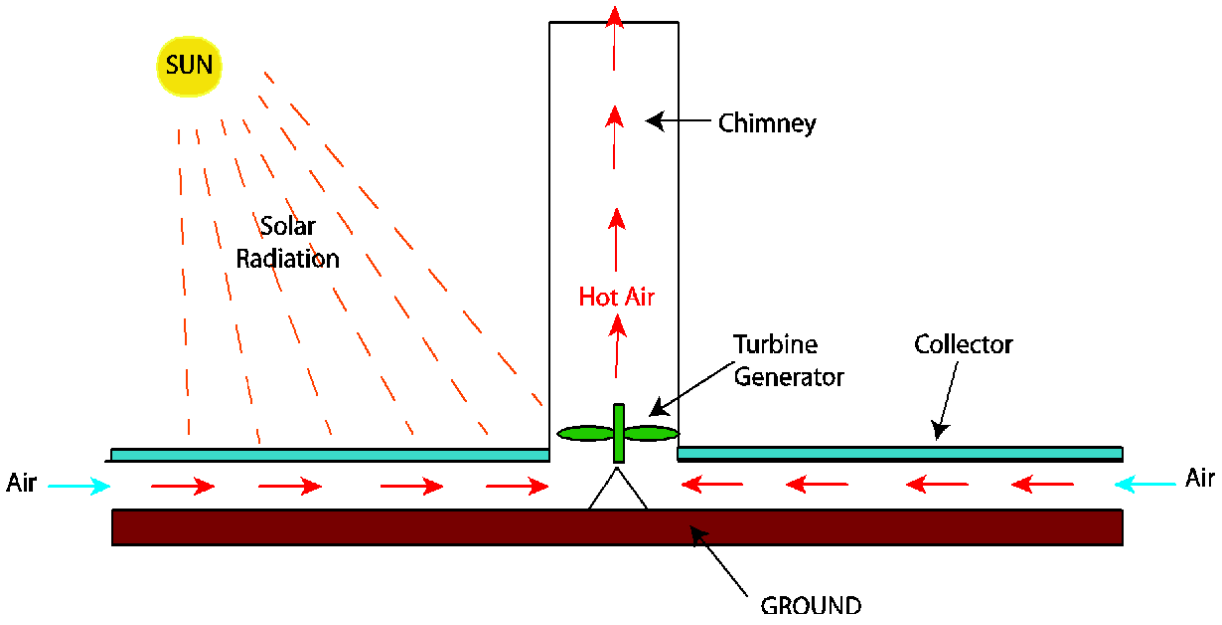

Figure 13: Solar Updraft Tower Schematic Diagram **[13]**

5. Literature review

The Solar Vortex Engine (SVE) seeks to substitute the tall and costly chimney structure in solar updraft power plants with a more compact and economical component known as the vortex generator. **[14]** employs Computational Fluid Dynamics (CFD) to simulate the entire SVE system, aiming to identify the optimal location for the turbine unit and demonstrate the vortex generator's capability to replace the traditional chimney. Three distinct cases for the SVE are analyzed and compared against corresponding cases of the Solar Chimney Power Plant (SCPP). The findings highlight that the most effective turbine location is at the outlet hole of the vortex generator. The outlet hole achieves an updraft air velocity of 1.82 m/s, surpassing the 1.56 m/s recorded at the base of a solar chimney with an equivalent diameter to the upper hole. Incorporating the turbine pressure drop does not compromise the formation and preservation of the air vortex. Consequently, the 1-meter-high vortex generator successfully replaces the 8.6-meter chimney component in solar updraft power plants, significantly reducing both the cost and construction complexity of the plant. Moreover, the vortex generator accelerates the air from the solar collector, enhancing its velocity by 14 times. The SVE's power output is directly correlated with the static pressure drop across the turbine. The mean difference values across the air vortex field between cases with and without a turbine are 0.67 Pa and 0.026 m/s for static pressure drop and velocity magnitude, respectively.

This study by **[15]** involves a two-dimensional numerical calculation of laminar airflow induced by natural convection within a solar chimney. The mathematical model employed encompasses continuity, momentum, and energy equations in a cylindrical coordinate system, applying Boussinesq's approximation. The simulation was executed using Comsol Multiphysics software. The outcomes revealed a significant correlation between the performance of the solar chimney, the Rayleigh number, and geometric properties such as the junction curvature radius and collector height.

In recent study done by **[16]** they did an analytic and numerical research conclude that utilizing solar chimney technology is a viable method for harnessing power from solar energy. In this study, an investigation was conducted by analyzing the weather map of Iran and employing GIS software to identify a suitable location for a solar power plant. Four distinct physical models for solar chimneys were proposed and examined. The study, conducted through numerical simulation using MATLAB, focused on these models within the city of Bam, located in Kerman province. The variability among the four solar chimney models lies in the storage system and the incorporation of an air diffuser. The behaviors of each model were scrutinized based on valid meteorological data collected on a specific day at the chosen site. The simulation results, encompassing airflow speeds in various internal sections of the chimney and the production capacity of each model, contribute to the identification of the most effective and suitable solar chimney model for the study site. This facilitates a reliable estimation of the final production output.

This investigation by **[17]** aims to empirically explore the impact of a divergent solar chimney in contrast to a cylindrical chimney on the performance of a solar chimney. Three scaled-down divergent solar chimney models, measuring 1 meter, 1.5 meters, and 2 meters, were

manufactured and subjected to testing under various simulated heat loads. The obtained results were juxtaposed with those from cylindrical solar chimneys of comparable heights. The experiments reveal that a divergent solar chimney enhances the theoretical power generation potential, augments the stack effect, and attains higher outlet velocities compared to a cylindrical solar chimney. The outlet temperature on the 2-meter divergent chimney was recorded at 341.3K, surpassing the 330.4K on the cylindrical chimney, indicating an improved stack effect. The highest average velocities in both the divergent and cylindrical chimneys were observed under an electric heat load of 2 kW at 0.994 m/s and 0.820 m/s, respectively, in the 1-meter configuration. Additionally, it was noted that the air velocity in a shorter divergent chimney is higher than in taller divergent chimney models, while still being superior to all cylindrical heights. This study concludes that a shorter divergent solar chimney yields greater energy production compared to a taller cylindrical solar chimney. Consequently, it becomes feasible to reduce the overall cost of a solar chimney by diminishing the height of the main structure without compromising the solar chimney's performance.

This paper published by **[18]** seeks to examine the experimental data derived from a divergent solar chimney, with the experiments conducted in an open atmosphere under sunlight. The airflow rates within the chimneys are evaluated with variations in the collector outlet height. The experimental findings indicate that a chimney with a greater collector opening outperformed other models. Additionally, computational analysis using the ANSYS Fluent software package was conducted, revealing that a collector opening of 2.5m is recommended for achieving higher mass flow rates and system efficiency.

This study done by **[19]** involves three-dimensional axisymmetric modeling and numerical simulations of a Solar Chimney Power Plant (SCPP). Utilizing CFD software, a numerical model is developed and validated against experimental data from the literature. The research investigates the effects of geometric parameters of the chimney and collector, as well as different configurations, on the SCPP's performance. The findings highlight the optimal configuration as a diverging chimney, leading to enhanced power generation. The study emphasizes the positive impact of increased chimney height and collector radius on power output and efficiency, with each factor having an optimal value when construction and material costs are considered. The chimney tower radius is identified as having the most significant impact on performance, while the collector height and inclination exhibit optimum values. Based on the results, the most efficient SCPP configuration includes a 3.5 m chimney height, 30 cm tower diameter, 400 cm collector diameter with a 6 cm height, and zero inclination angles. The study provides valuable insights for the design of a SCPP real-scale prototype, allowing for the selection of dominant performance parameters to meet maximum power requirements.

In a study done by **[20],** they have conducted numerical investigations to explore potential enhancements in the flow field and heat transfer characteristics of a prototype solar chimney designed for power generation. Our focus has been on passive flow control methods, and we have modeled three different schemes to boost the velocity magnitude at the chimney entrance. The first scheme assesses the impact of varying the number of turbulent

generators on the maximum flow speed achieved. The second scheme examines the influence of the throat area at the entrance of the chimney. The final scheme delves into the effects of incorporating rounded edges with different radii at the chimney entrance.

In this work by **[21]** involves the investigation of geometric parameters' influence on convection airflow within a solar chimney, focusing on a two-dimensional prototype model. The chosen boundary conditions replicate real-world scenarios. The mathematical model adopted comprises a system of partial differential equations, including the continuity, momentum, and energy equations, along with the standard k-ε turbulence model. Numerical simulations were executed using a commercial Computational Fluid Dynamics (CFD) code based on the finite volume method. The obtained results exhibit good agreement with both experimental and numerical data. The study scrutinizes the effects of tower and collector radius/heights on the aerodynamic structure, providing insights applicable to the design of novel solar chimney systems.

[22] Found that, developing a solar chimney with optimal efficiency necessitates a dependable model for estimating the airflow rate generated by the solar irradiation-induced heat. Current analytical models commonly overlook density variations, either throughout the entire channel or within the channel gap. This research introduces a plume model founded on energy balances and thermal boundary theory, accounting for density variations in both horizontal and vertical directions. Implicitly expressed as a function of heat flux, this plume model is easily solvable through straightforward iterations. The validity of the model was assessed using experimental data available in literature. The results demonstrate that the plume model surpasses existing analytical models in performance. Acknowledging the challenges associated with airflow measurement, we propose further tests and calibrations of the plume model using more concrete and accurate experimental data. Despite its simplicity, the plume model holds potential for inclusion in building simulation programs.

In this study done by **[23]** found that the impact of replacing the conventional cylindrical tower with a diffuser tower on the power output of the Manzanares Solar Chimney Power Plant has been examined. An estimation of the power output of the plant was conducted under the assumption that a diffuser tower was employed. To facilitate the implementation of the draft in the tower, an alternative structure is suggested, deviating from the conventional sheet steel ring structure.

A study by **[24]** details a numerical exploration of a conical collector solar chimney featuring specific dimensions. To examine the impact on air velocity distribution, a square cross-section glass spiral was incorporated into the collector. The findings reveal that, at inlet air velocities of Re=99945 and 499729, the spiral enhances velocity distribution by 11.57% and 12.82%, respectively. This improvement is expected to have a direct effect on the instantaneous electric power output achievable with such a device. The investigation utilized the CFD program FLUENT 14.5, employing the K-ε model.

In this combined experimental and numerical investigation done by **[25]** found that the impact of varying the reduction area of the solar collector was explored. The reduction area refers to alterations in the height of the glass cover from the absorbing plate (specified as

h1=3.8cm, h2=2.6cm, and h3=1.28cm). The numerical analysis utilized the ANSYS Fluent software package (version 14.0) to solve the governing equations. The objective of this study was to assess how changes in the reduction area height affect the design velocity (the velocity that propels the turbine blade at the chimney inlet). The findings indicate that the third height (h3=1.28cm) yields the most favorable outcome.

Chapter II

Mathematical model formulation

1. Introduction

This chapter introduces the physical issue through a system of partial differential equations (PDE) that describes the diffuser effect within the physical domain of a solar chimney, as depicted in cylindrical coordinates.

2. Problem description

Using the right assumption and the mathematical formalisms using the Boussinesq's approximation in order to identify and analyze the behavior of the diffuser effect in two-dimensional air updraft solar chimney. Both air temperature and velocity parameters were experimentally tested for different temporal and spatial sites.

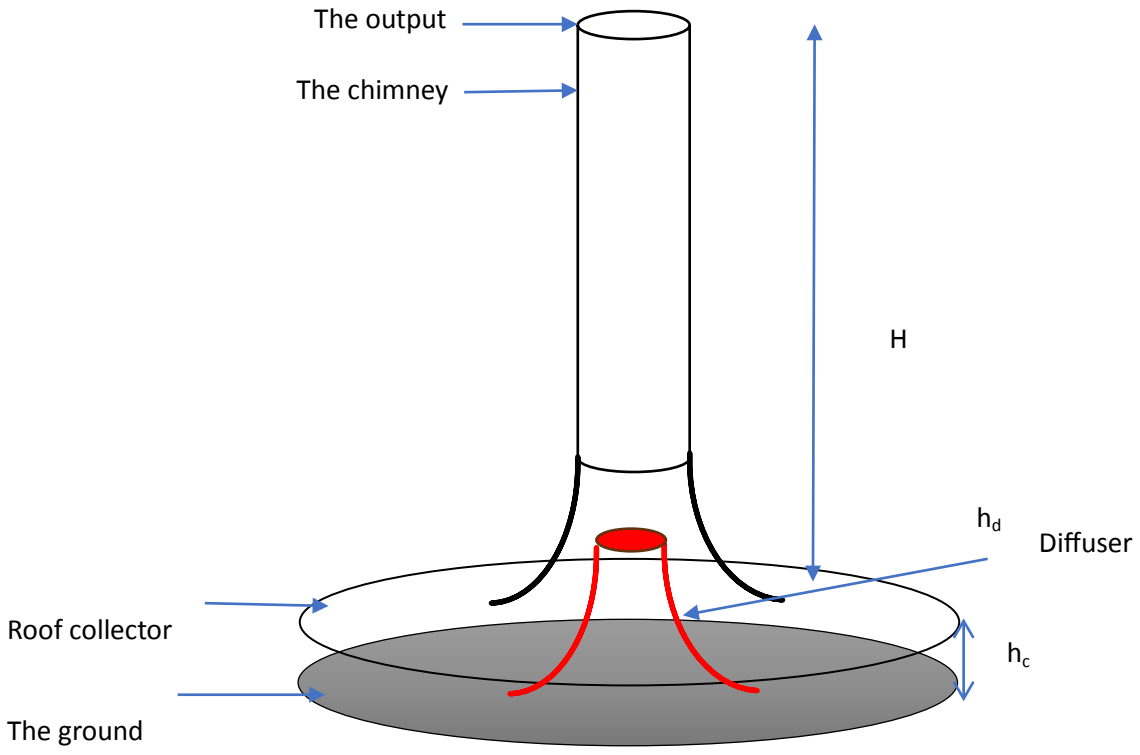

Figure 1: Solar chimney geometry

3. Mathematical model

Mathematical equations suitable for the geometry and flow conditions employed to describe the problem are:

3.1 Continuity equation:

$$\partial\rho/\partial t + \text{div}(\rho.\vec{V}) = 0 \quad (2.1)$$

Where:

ρ: Fluid density

$\vec{V}$: Velocity components

3.2 Momentum conservation equations:

$$\rho\left(\frac{\partial\vec{V}}{\partial t} + \left(\vec{v}.\overrightarrow{grad}V\right)\right) = -\vec{\nabla}p + \rho\vec{g} + \mu\Delta\vec{k} \quad (2.2)$$

3.3 Energy equation:

$$\frac{\partial T}{\partial t} + \left(\vec{V}.\overrightarrow{grad}\,T\right) = \frac{\lambda}{\rho Cp}\Delta T \quad (2.3)$$

4. Simplifying hypothesis:

- The flow is assumed to be permanent and laminar.
- The fluid is assumed to be Newtonian and incompressible.
- The flow is assumed to be axisymmetric where $(\frac{\partial}{\partial\theta}) = 0$.
- The conduction and the radiation through the collector are neglected.
- Viscous dissipation and pressure forces are neglected in the energy equation.
- The Boussinesq's approximation is used for the variations of the density in the terms of force of volume and directly correlated with temperature T. The reference temperature T_0 controls the fluid's physical characteristics, which are constant in the other terms of the equations;

$$\rho = \rho_0\,(1\text{-}\beta_T\,(T - T_0)) \quad (2.4)$$

Where:

$\beta_T = -\frac{1}{\rho_0}\frac{\partial P}{\partial T}$: The coefficient of thermal expansion

5. Mathematical modeling in cylindrical coordinates:

According to the above simplifying hypothesis, the continuity, momentum, and energy balance equations are reformulated as follows:

5.1 Continuity equation:

$$\frac{1}{r}\frac{\partial(rV_r)}{\partial r} + \frac{\partial V_z}{\partial z} = 0 \quad (2.5)$$

5.2 Momentum conservation equation:

$$\rho\left(V_r\frac{\partial V_r}{\partial z}\right) = -\frac{\partial p}{\partial r} + \mu\left(\frac{1}{r}\frac{\partial}{\partial t}\frac{\partial(rV_r)}{\partial r} - \frac{V_r}{r^2} + \frac{\partial^2 V_r}{\partial z^2}\right) \quad (2.6)$$

$$\rho\left(V_r\frac{\partial V_z}{\partial r}\right) = -\frac{\partial p}{\partial z}g_z\rho\beta_T(T - T_0) + \mu\left(\frac{1}{r}\frac{\partial}{\partial r}\frac{\partial(rV_z)}{\partial r} + \frac{\partial^2 V_z}{\partial z^2}\right) \quad (2.7)$$

5.3 Energy equation:

$$V_r\frac{\partial T}{\partial r} + V_z\frac{\partial T}{\partial z} = \frac{\lambda}{\rho C_p}\left(\frac{1}{r}\frac{\partial}{\partial r}\left(r\frac{\partial T}{\partial r}\right) + \frac{\partial^2 T}{\partial z^2}\right) \quad (2.8)$$

6. Boundary conditions

- At the air input: $T = T_c$, $V_r = 0$, $V_z = 0$
- At the output: $\frac{\partial V_z}{\partial z} = \frac{\partial V_r}{\partial z} = \frac{\partial T}{\partial z} = 0$
- Boundary Conditions for the ground: $T_{ground} = T_h$, $V_r = 0$, $V_z = 0$
- Boundary Conditions for the collector: $T = T_c$, $V_r = 0$, $V_z = 0$

7. Dimensionless mathematical model

It's suitable to use dimensionless model equations in order to discretize them using a numerical method and to make appearing the controlling parameters as the Rayleigh and Prandtl numbers. In this study the simulation software uses the finite elements method. Variables are considered as following:

$$r^+ = \frac{r}{D}, z^+ = \frac{z}{D}, T^+ = \frac{T - T_c}{T_h - T_c}, P^+ = \frac{P}{\rho(\alpha/D)^2}$$

$$V_r^+ = \frac{V_r}{(\alpha/D)}, V_z^+ = \frac{V_z}{(\alpha/D)}$$

7.1 Continuity equation:

$$\frac{1}{r^+}\frac{\partial(r^+V_r^+)}{\partial r^+} + \frac{\partial V_z^+}{\partial z^+} = 0 \quad (2.9)$$

7.2 Momentum conservation equation:

$$V_r^+\frac{\partial V_r^+}{\partial r^+} + V_z^+\frac{\partial V_r^+}{\partial z^+} = -\frac{\partial p^+}{\partial r^+} + P_r\left(\frac{1}{r^+}\frac{\partial}{\partial r^+}\frac{\partial(r^+V_r^+)}{\partial r^+} - \frac{V_r^+}{r^{+2}} + \frac{\partial^2 V_r^+}{\partial z^{+2}}\right) \quad (2.10)$$

$$V_z^+\frac{\partial V_z^+}{\partial r^+} + V_z^+\frac{\partial V_z^+}{\partial z^+} = -\frac{\partial p^+}{\partial z^+} + P_r\left(\frac{1}{r^+}\frac{\partial}{\partial r^+}\frac{\partial(r^+V_z^+)}{\partial r^+} + \frac{\partial^2 V_z^+}{\partial z^{+2}}\right) + R_a\,.P_r\,.\,T^+ \quad (2.11)$$

7.3 Energy equation:

$$V_r^+\frac{\partial T^+}{\partial r^+} + V_z^+\frac{\partial T^+}{\partial z^+} = \frac{1}{r^+}\frac{\partial T^+}{\partial r^+} + \frac{\partial^2 T^+}{\partial r^{+2}} + \frac{\partial^2 T^+}{\partial z^{+2}} \quad (2.12)$$

8. Dimensionless boundary conditions:

- At the air input: $T^+ = 0, V_r^+ = 0, V_z^+ = 0$

- At the output: $\frac{\partial V_z^+}{\partial z^+} = \frac{\partial (V_r)}{\partial x} = \frac{\partial T^+}{\partial z^+} = 0$

- Boundary Conditions for the ground: $T_h^+ = 1, V_r^+ = 0, V_z^+ = 0$

- Boundary Conditions for the collector: $T_c^+ = 0, V_r^+ = 0, V_z^+ = 0$

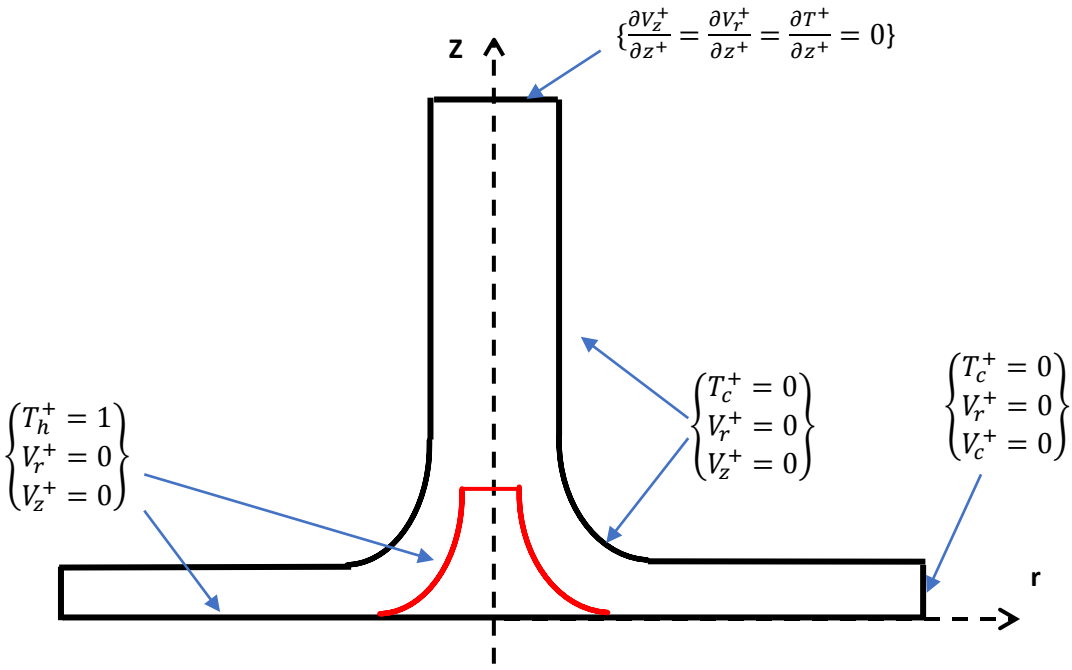

Figure 2: Dimensionless boundary conditions

CHAPTER III

NUMERICAL SIMULATION SOFTWARE

1. Introduction:

Numerical simulation software represents a pivotal tool in modern engineering, scientific research, and various industries. This software enables the modeling and analysis of complex systems and phenomena through computational methods, offering insights and predictions that might be challenging or impossible to attain through traditional experimental approaches alone. By leveraging mathematical algorithms and computational techniques, numerical simulation software can replicate real-world scenarios, allowing researchers and engineers to explore and understand intricate processes in fields such as fluid dynamics, structural mechanics, electromagnetics, and more. These simulations can range from simulating the behavior of airflow around an aircraft wing to predicting the structural integrity of a building subjected to seismic forces. One of the primary advantages of numerical simulation software is its ability to rapidly iterate and test different scenarios without the need for costly and time-consuming physical prototypes. This accelerates the design process, enhances product development cycles, and ultimately leads to more efficient and optimized solutions. Moreover, numerical simulation software empowers researchers to investigate phenomena that are difficult or unsafe to replicate in a laboratory setting, such as extreme weather conditions, astronomical events, or the behavior of materials under extreme pressure or temperature. In addition to its application in engineering and science, numerical simulation software also finds utility in fields like medicine, finance, and environmental science, where it aids in modeling biological processes, predicting market trends, or simulating the impact of human activities on ecosystems. Overall, numerical simulation software plays a vital role in advancing knowledge, driving innovation, and solving complex problems across a diverse range of disciplines, making it an indispensable tool in the modern era of technology and discovery.

2. COMSOL software overview:

COMSOL Multiphysics is a powerful numerical simulation software package that enables engineers, scientists, and researchers to model and simulate a wide range of physical phenomena across various fields and disciplines. It stands out for its versatility in handling coupled physics phenomena, meaning it can simulate interactions between different physical processes simultaneously.

Here's an overview of some key features and capabilities of COMSOL Multiphysics:

1-Multiphysics Simulation

2-Customizable Physics Interfaces

3-Geometry Modeling

4-Mesh Generation

5-Solver Technology

6-Post-Processing and Visualization

7-Application Builder

8-Multiphysics Coupling

3. Software computation process

3.1 Phase 1: Model selection

In this phase, we begin by choosing the suitable mode and spatial dimensions, which, in our scenario, is 2D. Next, we specify the variables from the Multiphysics options. Then, we proceed by selecting the Model Navigator button. In our context, the model tree is displayed, showcasing the relevant components and settings.

1-Incompressible Navier-Stocks (ns)

2-Convection and Conduction (cc)

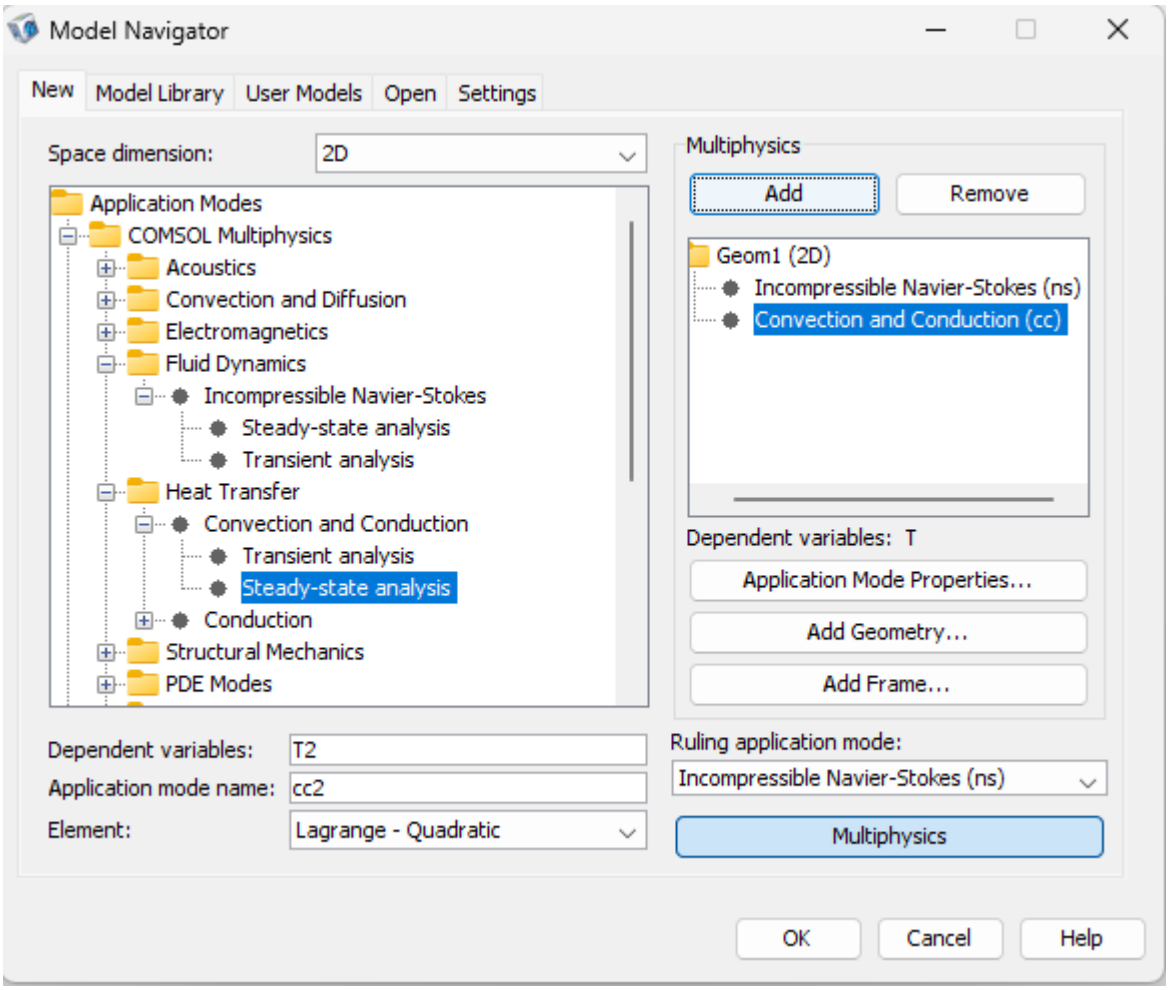

Figure 1: Model navigator window

3.2 Phase 2: Geometry creating

During this phase, the physical design is executed utilizing the CAD tools accessible on the draw menu. Lines and curves are chosen, each assigned with suitable coordinates, and subsequently linked with each other to generate the chimney and diffuser geometry.

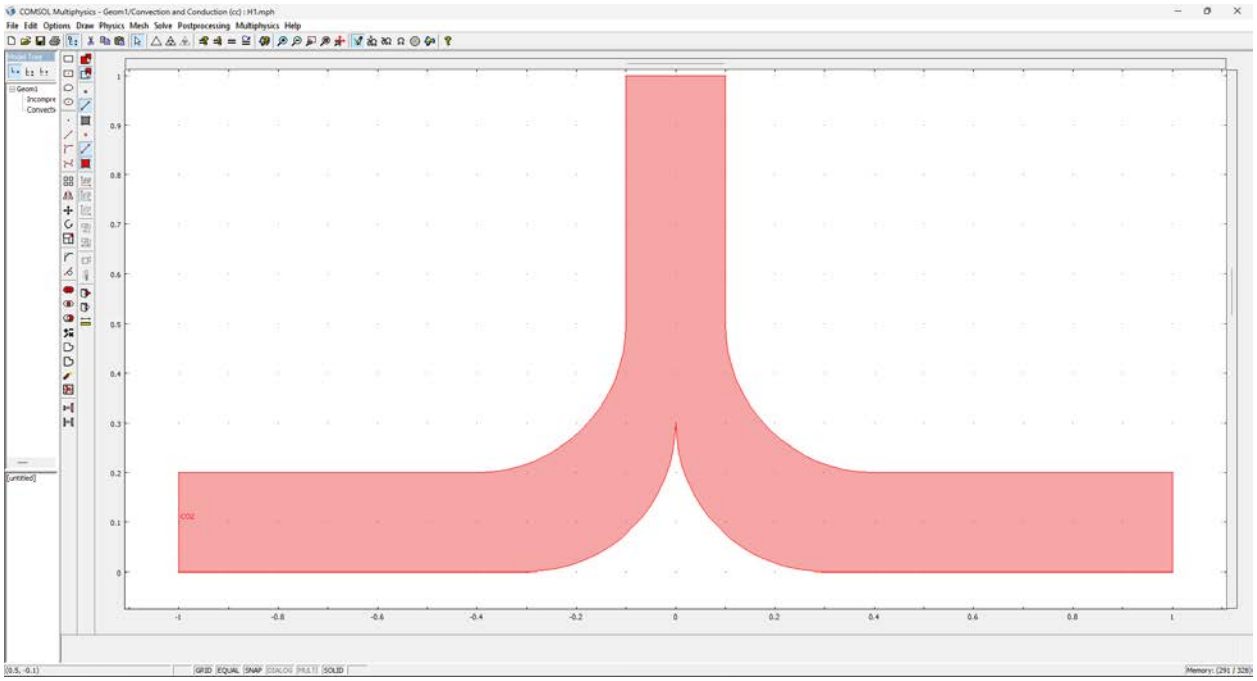

Figure 2: Geometry creation

3.3 Phase 3: Constant input

By heading to **Options** then **constants**

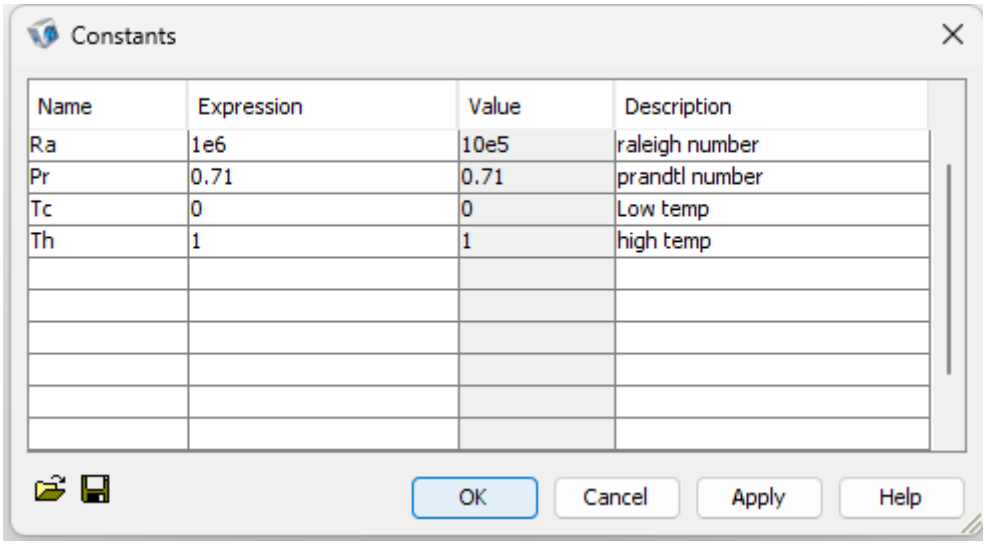

Figure 3: Constant table

3.4 Phase 4: Defining the physics

This phase involves establishing all the parameters and equations governing the physics within the model.

Physics→ Subdomain setting: select subdomain and then define the fluid properties (in our case it is dimensionless)

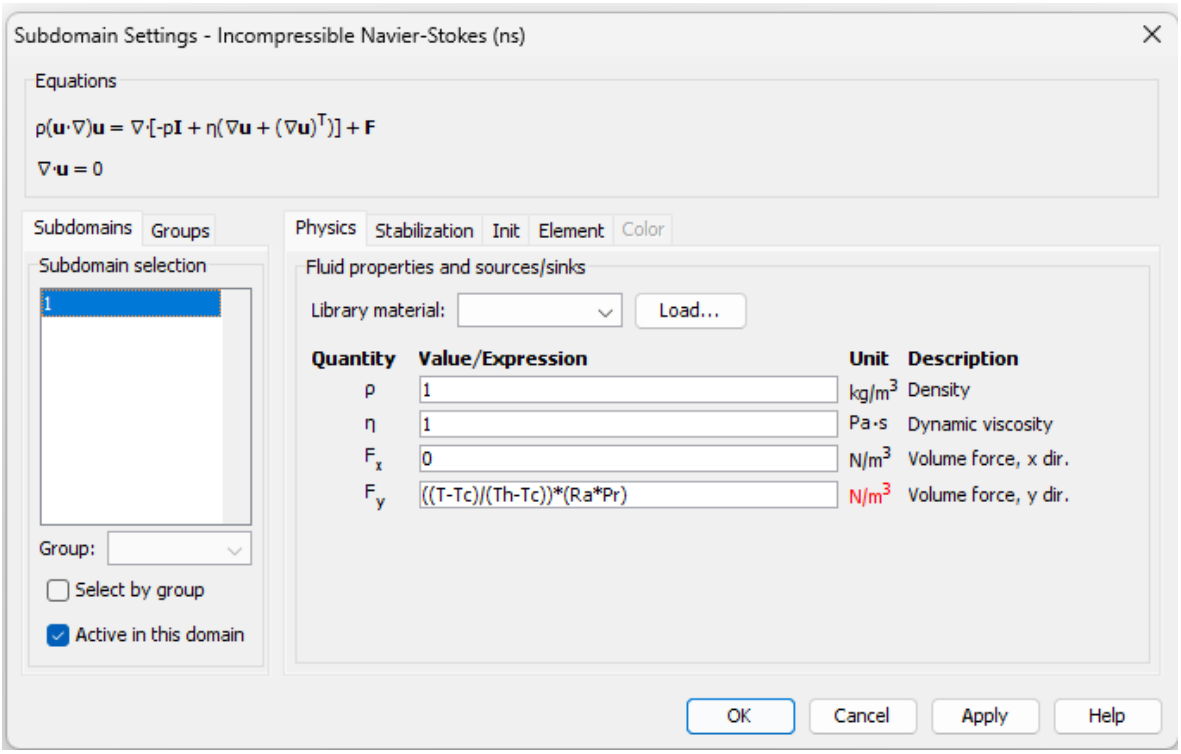

Figure 4: Subdomain setting window in the Navier-stocks mode

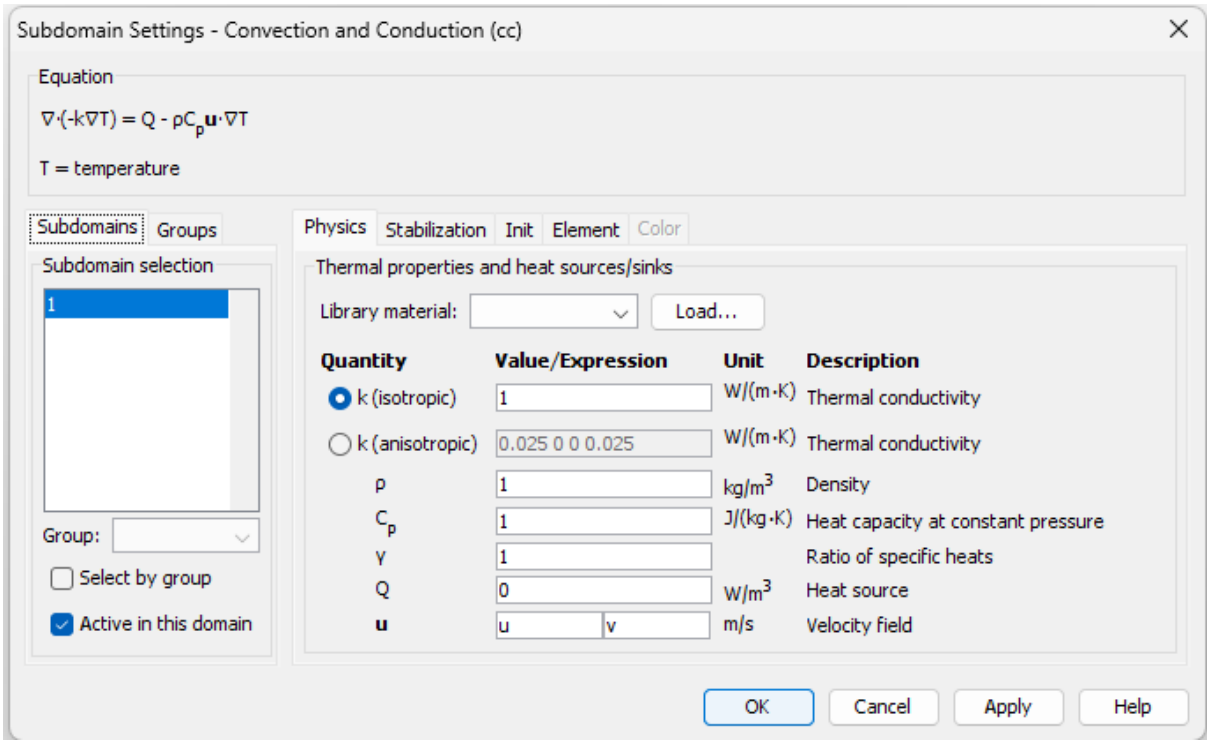

Figure 5: Subdomain setting in the convection and conduction mode

Physics→ Boundary condition: Boundary conditions for each border will be specified using the Boundary Settings window, followed by confirmation of the selection.

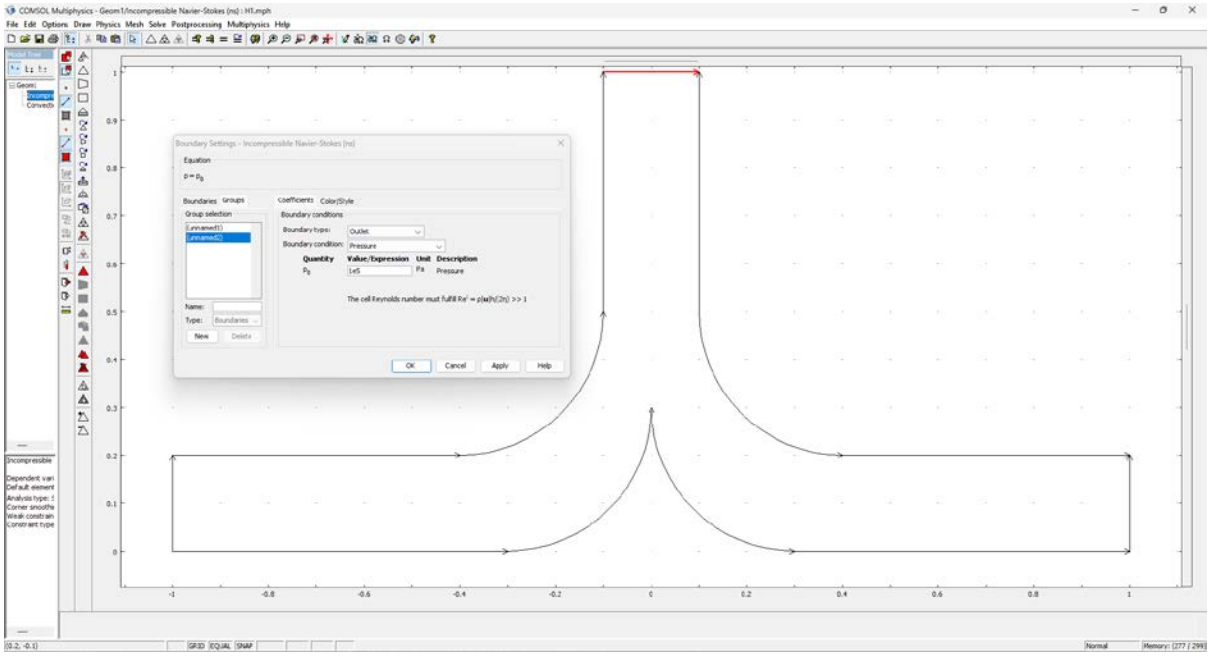

Figure 6: Boundary conditions in Incompressible Navier-stokes mode for the outlet

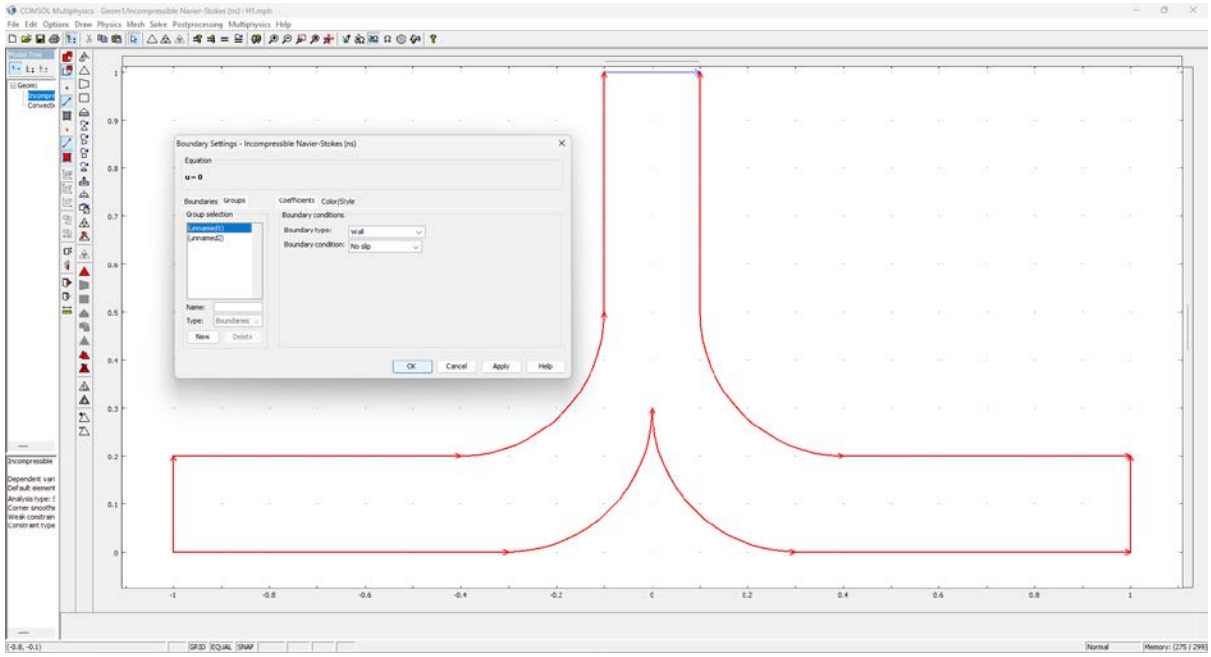

Figure 7: Boundary conditions in Incompressible Navier-stokes mode for the walls

Phase 5: Meshing the geometry

Choose "Mesh" from the toolbar then proceed to initialize the mesh, refine it, and refine the selection.

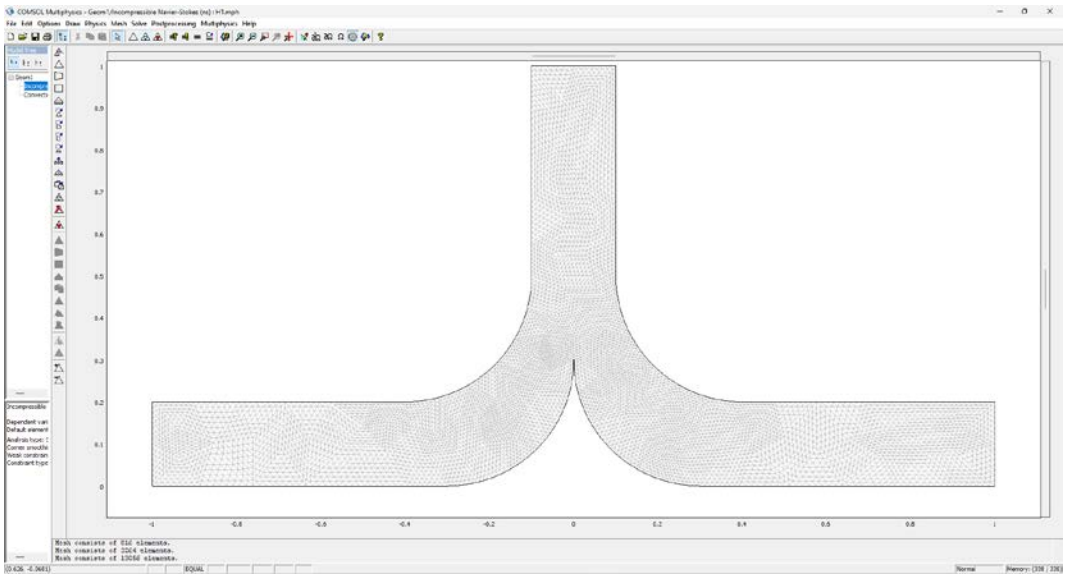

Figure 8: Refined mesh window

3.6 Phase 6: Solving the model

We adjusted specific solver properties within the Solver Parameters menu.

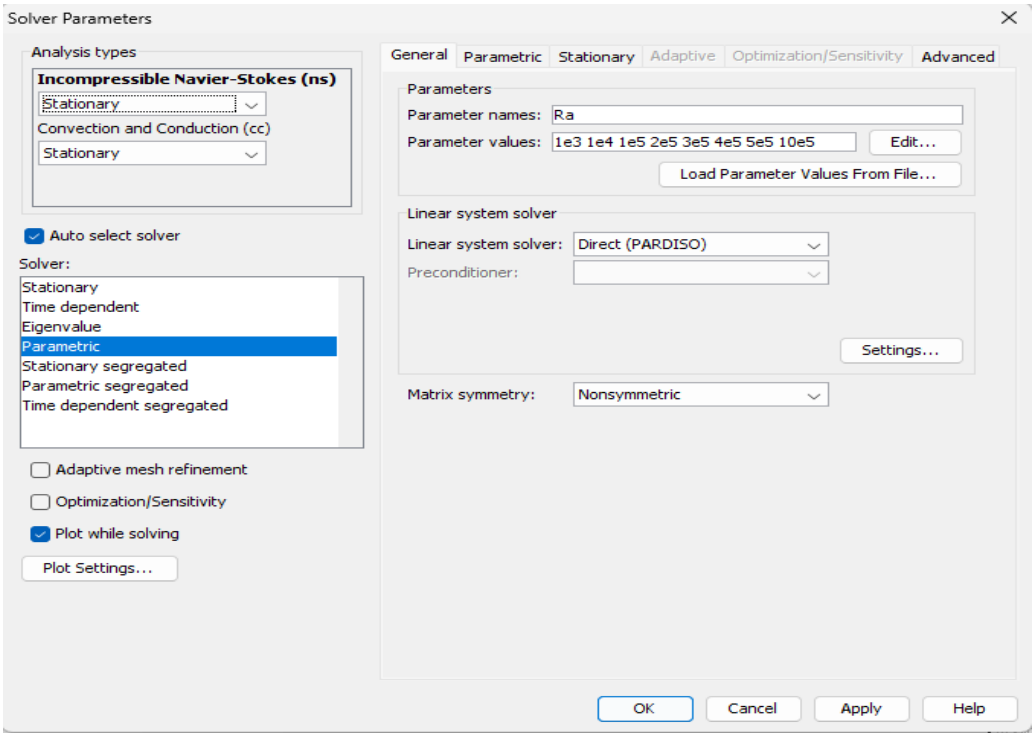

Figure 9: Solver parameters window

3.7 Final phase : Post processing and plotting

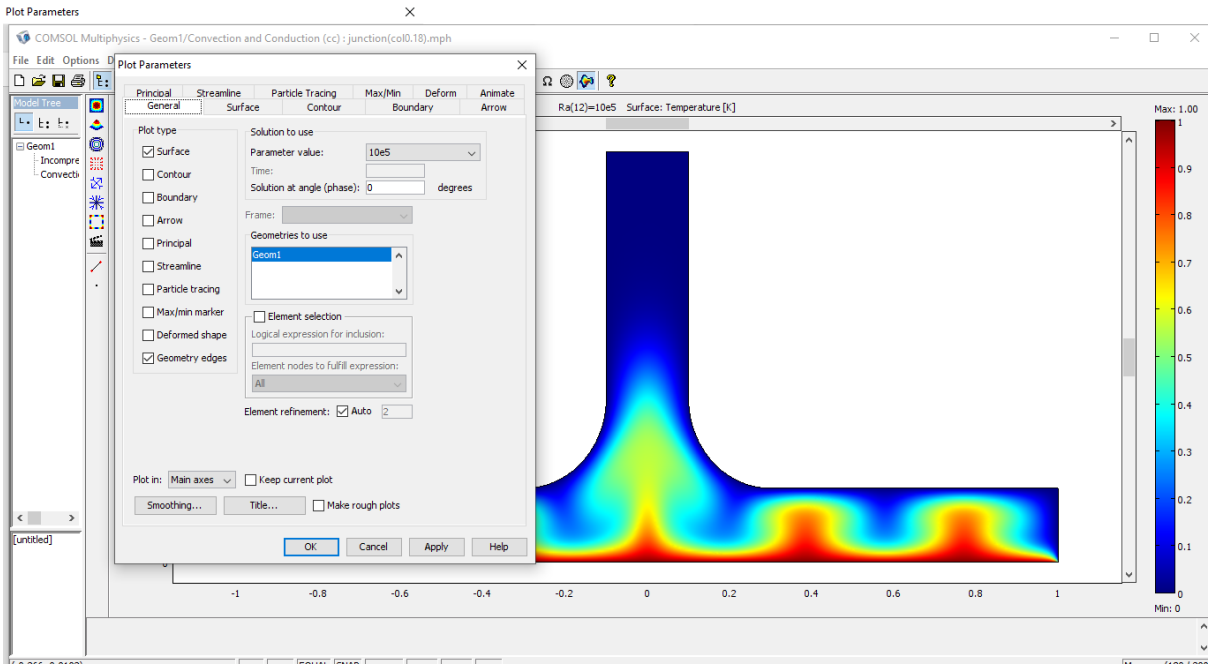

Figure 10: Post processing and outcome visualization

CHAPTER IV

RESULTS AND DISCUSSION

1. Introduction:

This chapter presents the findings of the study, focusing on the impact of geometric parameters of the diffuser on the development of airflow within the solar chimney. These findings are depicted through isolines of dimensionless velocity and temperature, along with profiles of the vertical velocity component, which directly influences the turbine to produce power.

2. The impact of the diffuser on the isolines of temperature and velocity with Ra=5x10^5:

2-1 Without diffuser $h_d/h_c = 0$

This observation suggests a fully developed natural convection throughout the entire system. This is manifested as a distortion or warping of the isothermal lines, which are lines of constant temperature, across the entire system. This distortion indicates a change in the temperature distribution, which is a direct result of the increased natural convection. Figure 1 provides more detailed view of this phenomenon. It illustrates an intensified presence of counter-rotating cells at the top of the chimney's entrance. These counter-rotating cells are areas where the air circulates in opposite directions. This circulation is mediated by a primary cell that is moving upwards. The upward movement of this primary cell is critical as it represents the generation of airflow under a convective mode. In the context of a solar chimney, this convective mode is crucial. The heat from the sun warms the air inside the chimney, causing it to rise (due to the buoyancy effect). As the warm air rises, it creates a pressure difference that drives the airflow. This airflow can then be used to turn a turbine and generate power. Therefore, the observation of an increase in natural convection, as indicated by the distortion of the isothermal lines and the intensification of the counter-rotating cells in figure 2, is a positive indication of the system's performance. It suggests that the solar chimney is effectively harnessing the sun's heat to generate a strong, sustainable airflow. This, in turn, can lead to more efficient power generation.

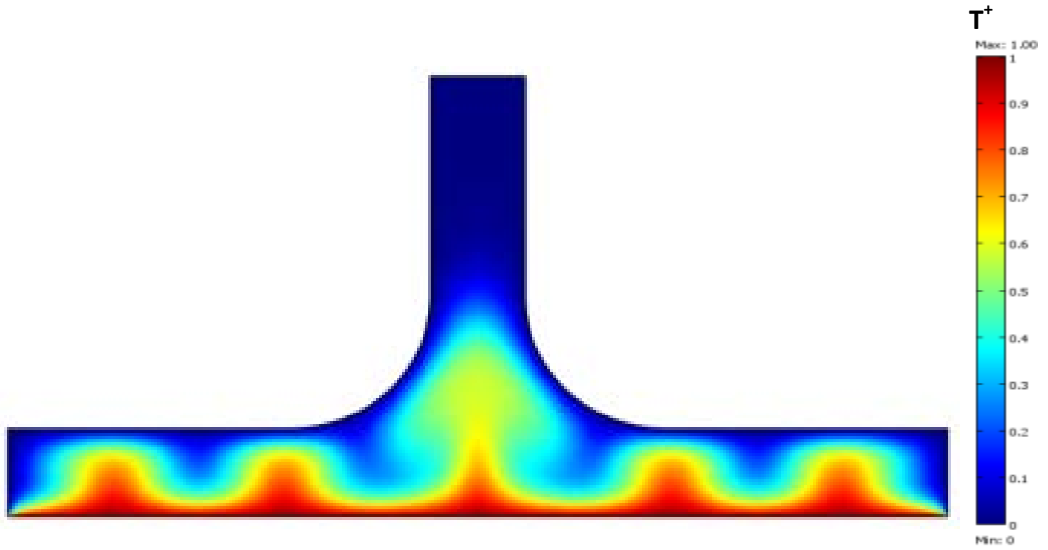

Figure 1: Dimensionless temperature distribution without diffuser ($h_d/h_c = 0$) and Ra=5x10^5

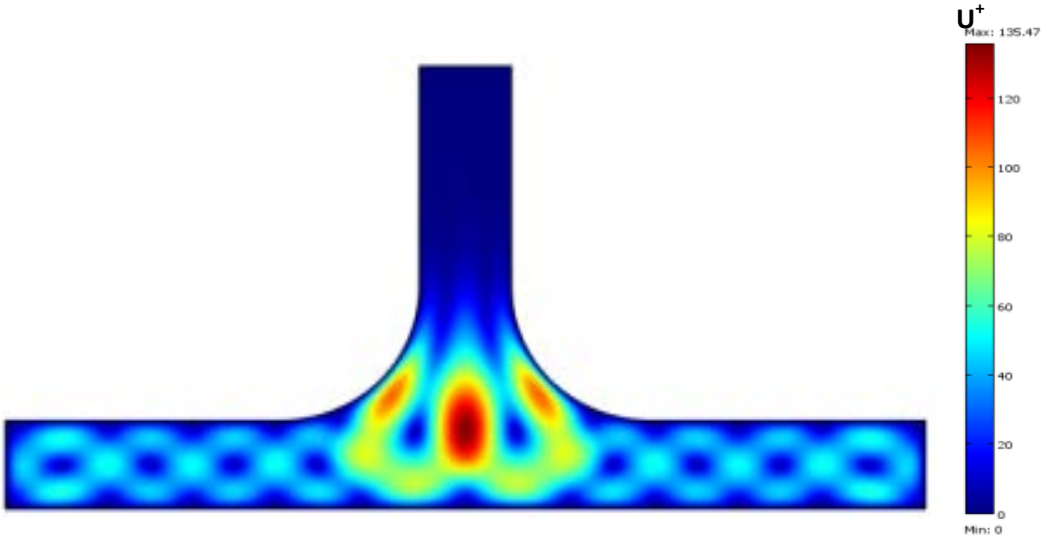

Figure 2: Dimensionless velocity field without diffuser ($h_d/h_c = 0$) and Ra=5x10^5

2-2 Effect of a Diffuser with height ratio $h_d/h_c = 0.5$

In figure 3, we observe the isotherms for a Rayleigh number (Ra) of 5×10^5. Isotherms are lines that connect points of equal temperature, and they provide a visual representation of the temperature distribution within a system. In this case, the isotherms are showing us how heat is distributed within the solar chimney. The deformation of natural convection throughout the entire system is suggested by the warping of these isothermal lines. Natural convection is a mode of heat transfer where fluid motion is generated by differences in fluid density, which are caused by temperature gradients. In simpler terms, hot (less dense) air rises, and cold (more dense) air sinks. The warping of the isothermal lines indicates that this natural convection process is being distorted or changed in some way. Moving on to figure 4, it illustrates an intensified presence of counter-rotating cells at the top of the chimney's entrance due to installation of a diffuser in this area. These counter-rotating cells are more closed but with less velocity due to the area restriction around the diffuser. As we can notice the dimensionless velocity U^+ has decreased from 135.74 in the case of no diffuser to 106 with a diffuser at a ratio of $h_d/h_c = 0.5$**.** This decrease is mainly due to the space restriction caused by the diffuser, as the natural convection require enough free space for its development, the diffuser in this case will slow down the intensification of the airflow.

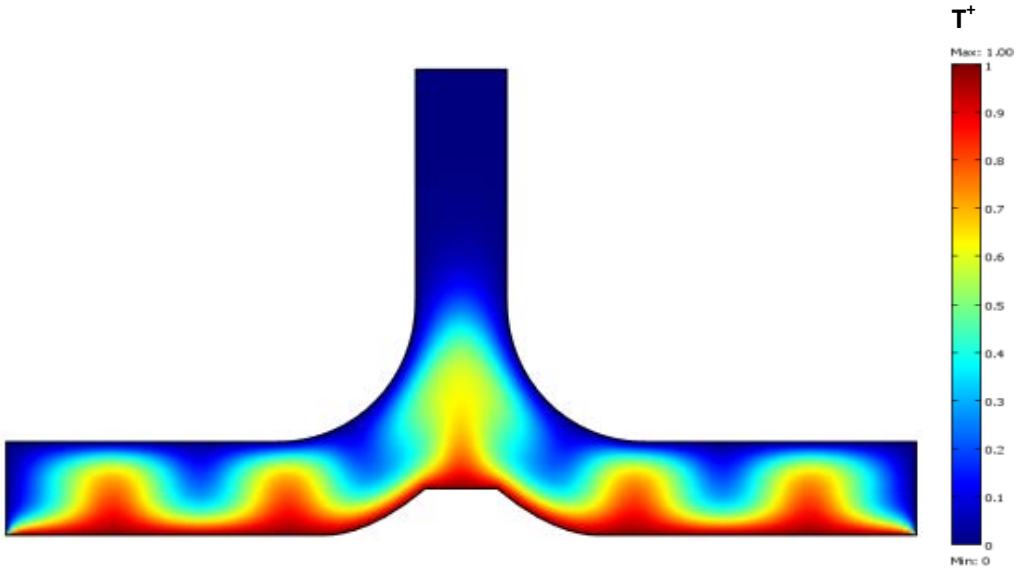

Figure 3: Dimensionless temperature distribution with diffuser ($h_d/h_c = 0.5$) and Ra=$5x10^5$

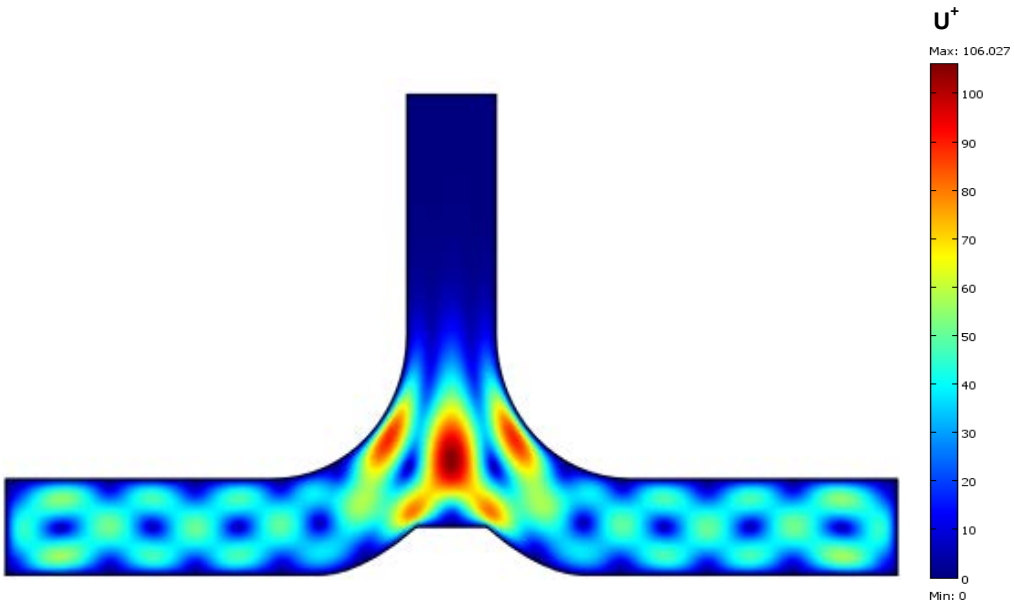

Figure 4: Dimensionless velocity field with diffuser ($h_d/h_c = 0.5$) and Ra=5x10^5

2.3 Diffuser with height ratio $h_d/h_c = 1$

Figure 5 shows isotherms for Ra= 5×10^5 in the case of diffuser height h_d/h_c=1 where we can see a complete distortion of the isothermal lines, which are lines connecting points of equal temperature, is observed. This distortion is a clear demonstration of the dominance of natural convection heat transfer within the system. At the entrance of the chimney, there is a noticeable airflow, indicating that the system is effectively drawing air into the chimney. In figure 6 which represent the airflow velocity distribution there is no change under the collector area, which is the part of the solar chimney where solar radiation is converted into thermal energy. Contrary, in the junction area of the chimney a noticeable change has occurred in the airflow due to the convective cells fusion from 5 small cells in figure 4 to 3 big cells in the entrance area of the chimney. The increase of the diffuser height has impacted the airflow negatively by reducing its intensity represented by the dimensionless air velocity U^+ from 106 to 87.

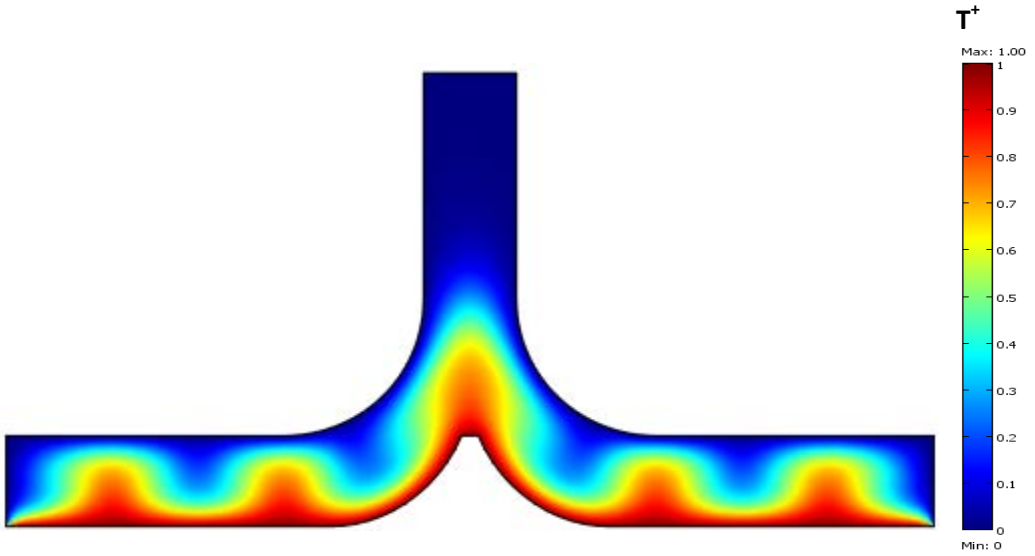

Figure 5: Dimensionless temperature distribution with diffuser ($h_d/h_c = 1$) and $Ra=5x10^5$

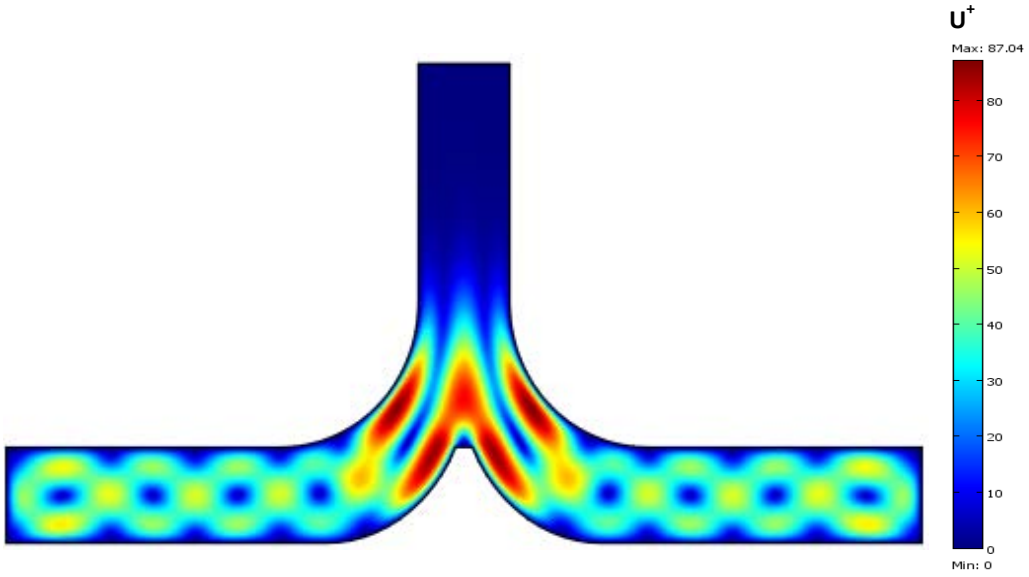

Figure 6: Dimensionless velocity field with diffuser ($h_d/h_c = 1$) and $Ra=5x10^5$

2-4 Diffuser with $h_d/h_c = 1.5$

We can see in figures 7 and 8, the isothermal and velocity lines where we notice that isothermal lines distribution is similar to the previous figures for different diffuser heights. But when we observe the figure 8 we notice a significative change qualitatively and quantitatively. The counter-rotating cells split up and became four main cells, two in each side of the chimney with a slight increase in the maximum dimensionless resultant velocity U^+.

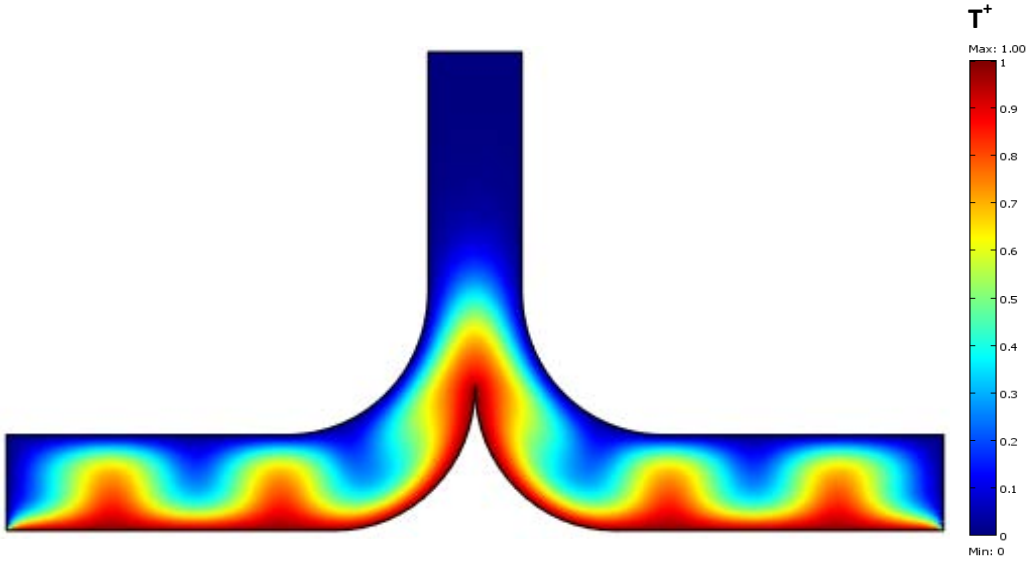

Figure 7: Dimensionless temperature distribution with diffuser (h_d/h_c = 1.5) and Ra=5x10^5

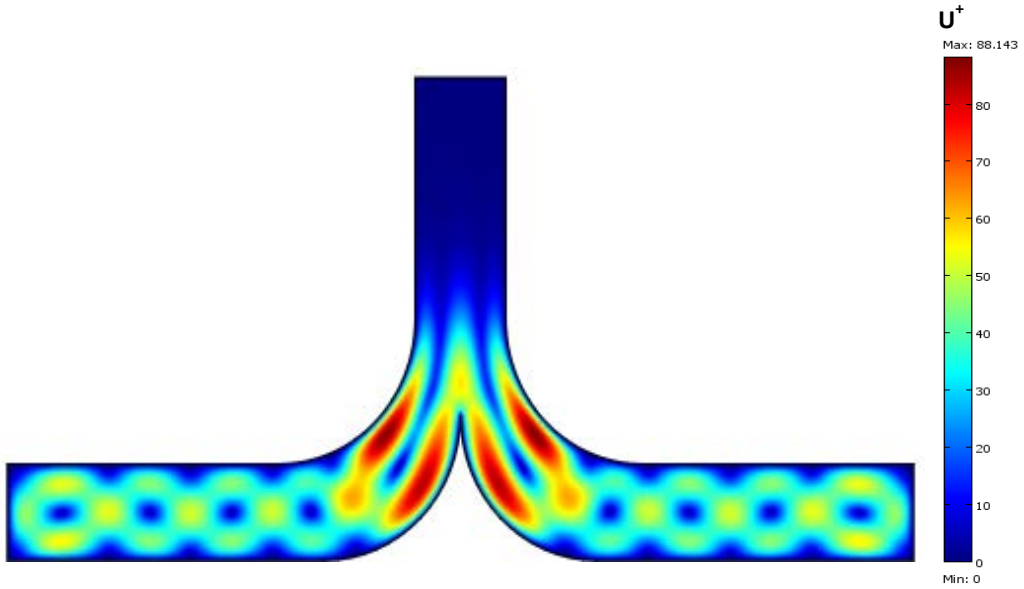

Figure (8): Dimensionless velocity field with diffuser (h_d/h_c = 1.5) and Ra=5x10^5

3. Effect of Rayleigh number on airflow vertical velocity:

In figure 9, a series of plots carefully delineate the dimensionless vertical velocity profiles of air under various values of the Rayleigh number while maintaining a constant diffuser height with an aspect ratio equal to 1. This reveals that the velocity exhibits an increasing evolution proportional to the Rayleigh number which is obvious because the natural convection is controlled and measured by the Rayleigh number value, more the value is high more the convection is developed and vice versa.

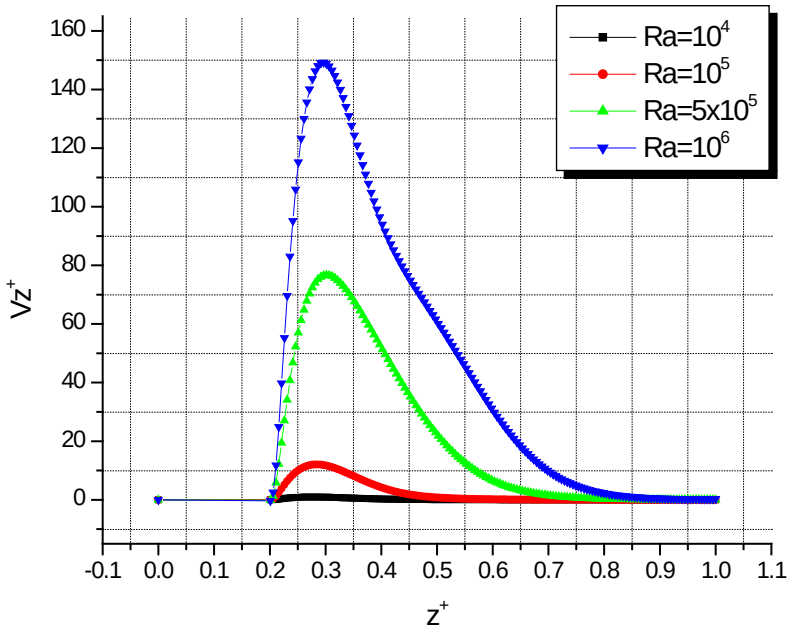

Figure 9: Dimensionless vertical velocity (V_z^+) for different Ra values with diffuser ($h_d/h_c = 1$)

4. Effect of the diffuser height on airflow vertical velocity:

Examining figure 10, which showcases dimensionless vertical airflow velocity profiles across various diffuser heights while maintaining a fixed Rayleigh value of $Ra=5.10^5$, we discern a notable trend. Elevating the diffuser height slow down the development of airflow throughout the space, this is resulting in a progressive decrease in velocity magnitude. Illustratively, considering the case without diffuser, the dimensionless vertical velocity peak

registers at 140, compared to a peak around 55 observed for a height ratio of 1.5. This height differential yields a substantial enhancement the smoothness flow path but in the same time to reduce the amplitude of the airflow velocity. In addition, the use of a diffuser with a right height divides the flow in two main regions of a potential turbine spot instead of one in the case of a chimney without diffuser.

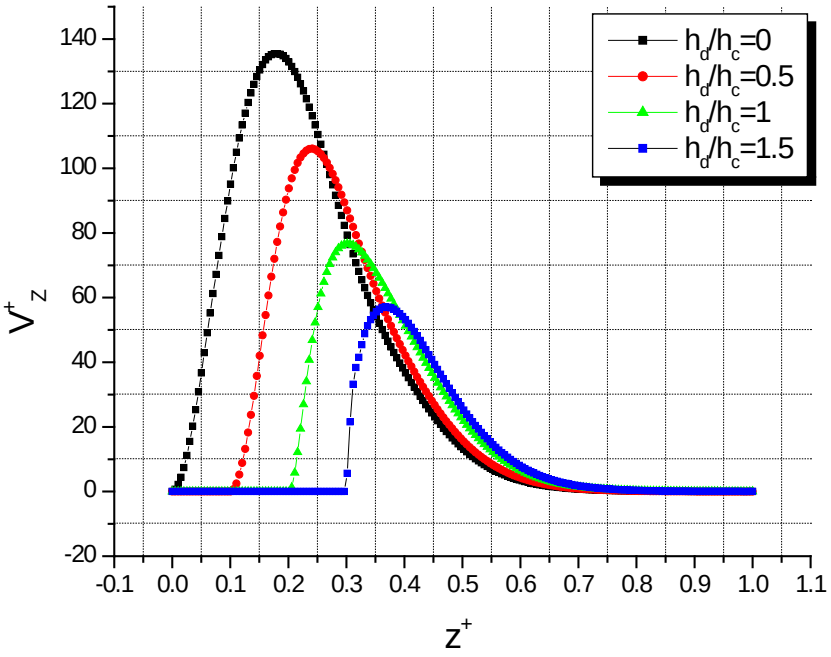

Figure 10: Dimensionless vertical velocity (V_z^+) for different height ratio (h_d/h_c) with Ra=5x10^5

Conclusion

In our parametric study, we performed a numerical simulation of an axisymmetric solar chimney using COMSOL Multiphysics software. The objective was to simulate the airflow velocity and structure resulting from natural convection within the solar chimney. To achieve this, we applied the Boussinesq approximation and made relevant assumptions. These assumptions encompassed laminar fluid flow, steady-state conditions, Newtonian behavior, and incompressibility. Additionally, we formulated the mathematical equations using a partial differential equation (PDE) system in cylindrical coordinates.

We investigated the impact of the diffuser height on natural convection within the solar chimney. Our findings revealed that a solar chimney with no diffuser h_0=0 provides the optimal geometry for achieving the highest efficiency at maximum vertical velocity. We concluded that the solar chimney's performance is closely tied to the variation in diffuser height.

Our study on the diffuser's height demonstrated that decreasing it facilitates smoother and more rapid airflow development throughout the entire solar chimney. Furthermore, this research enabled us to pinpoint the optimal location for the turbines, ensuring maximum efficiency.

The use of a diffuser for the case of buoyancy-driven airflow is constraining the flow and dividing it on two main regions for the turbines placement instead of only one optimal spot for one turbine but with a higher driving air velocity.

References

[1] www.sbp.de 26/12/2023

[2] https://en.wikipedia.org/wiki/File:Solar_Chimney_Manzanares-view_of_the_tower_through_the_collector_glass_roof.JPG 26/12/2023

[3] https://www.solarpanelsindustry.com/2012/06/solar-chimney-turbine.html 26/12/2023

[4] Siyang Hu, Dennis Y.C. Leung, John C.Y. Chan Numerical modelling and comparison of the performance of diffuser-type solar chimneys for power generation https://www.elsevier.com/locate/apenergy

[5] Filkoski, Risto V. & Stojkovski, Filip & Stojkovski, Valentino. (2013). A CFD study of a solar chimney power plant operation. 2

[6] Cristiana B. Maiaa, Felipe V.M. Silvaa , Vinícius L.C. Oliveiraa , Lawrence L. Kazmerskia An overview of the use of solar chimneys for desalination, www.elsevier.com/locate/solener

[7] https://en.wikipedia.org/wiki/Solar_chimney 26/12/2023

[8] https://www.mdpi.com/2071-1050/14/14/8839 26/12/2023

[9] https://www.sbp.de 26/12/2023

[10] https://spectrum.ieee.org/will-balloons-boost-the-solar-updraft-tower-idea 26/12/2023

[11] : https://www.nationalgeographic.com/history/article/140416-solar-updraft-towers-convert-hot-air-to-energy 26/12/2023

[12] https://www.sbp.de/en/ 26/12/2023

[13] J. H. Y. Too and C. S. N. Azwadi Numerical Analysis for Optimizing Solar Updraft Tower Design Using Computational Fluid Dynamics (CFD) 10.

[14] Tukkee A.M., Al-Kayiem H.H., Gilani S.I.U. Assessment of the Turbine Location for Optimum Performance of the Solar Vortex Engine as a Replacement to the Tall Chimney Solar Updraft Power Plant Design, J. Appl. Comput. Mech., 10(1), 2024, 38–54. https://doi.org/10.22055/jacm.2023.43942.4146

[15] Brahimi Nouha (2023) Numerical computation of geometric parameters effects on the solar chimney performance (master's thesis)

[16] Amir Bagheran Sharbaf*, Ali Asghar Shojaei, Paniz Bagheran Sharbaf Analysis of Solar Chimney Power Plants Based on the Bam's Climate (2021) https://doi.org/10.31803/tg-20200527124037

[17] Billal Belfegas , Salah Larbi , Tahar Tayebi Experimental and Theoretical Investigation on a Solar Chimney System for Ventilation of a Living Room (2021) https://doi.org/10.18280/mmep.080213

[18] N Rajamurugu 2021 IOP Conf. Ser.: Earth Environ. Sci. 850 012008

[19] Ekin Ozgirgin Yap, Ece Ayli, Osama Nsaif Numerical investigation on the performance of a small-scale solar chimney power plant for different geometrical parameters (2020) www.elsevier.com/locate/jclepro

[20] Alaa Ismail, Abd-Allah El-Marhoumy, A. M. Hamed2 and A. M. T. A. Eldein Hussin NUMERICAL MODELING FOR A SOLAR CHIMNEY (2019)

[21] Badia Ghernaout, Said Bouabdallah, Mohammed El Hadi Attia, Müslüm Arıcı, Zied Driss Parametric Study of the Airflow Structure in a Solar Chimney (2020)

[22] Guoqing He, Jianshun Zhang, Shiyi Hong A new analytical model for airflow in solar chimneys based on thermal boundary layers (2016) www.elsevier.com/locate/solener

[23] Pranav S. Sawant, Aniket A. Gor EFFECT OF A DIFFUSER TOWER ON THE POWER OUTPUT OF A SOLAR CHIMNEY POWER PLANT (2016) https://www.researchgate.net/publication/301287134

[24] Farhan Lafta Rashid, Salah Noori Alnomani EFFECT OF SPIRAL RIB ON SOLAR CHIMNEY COLLECTOR PERFORMANCE (2016).

[25] Aseel K. Shyaa Rafea A. H. Albaldawi Maryam Muayad Abbood Experimental and Numerical Study of Collector Geometry Effect on Solar Chimney Performance (2016) http://dx.doi.org/10.22153/kej.2016.05.002

Abstract

This study focuses on a two-dimensional numerical analysis of laminar airflow resulting from natural convection within a solar chimney. The mathematical model relies on the continuity, momentum, and energy equations formulated in a cylindrical coordinate system, incorporating the Boussinesq approximation. The simulation was executed using COMSOL Multiphysics software. Notably, our findings revealed a strong correlation between the solar chimney's performance and the diffuser height.

Keywords: Natural convection, solar chimney, Boussinesq's approximation, numerical simulation.

ملخص

هذه الدراسة تركز على تحليل عددي ثنائي الأبعاد لتدفق الهواء اللامتساوي الناتج عن التسخين الطبيعي داخل مدخنة شمسية. يعتمد النموذج الرياضي على معادلات الاستمرارية والزخم والطاقة المصاغة في نظام إحداثيات أسطواني، مع استخدام تقريب بوسينيسك.

تم تنفيذ المحاكاة باستخدام برنامج Comsol Multiphysics ومن الجدير بالذكر أن نتائجنا أظهرت ترابطًا قويًا بين أداء المدخنة الشمسية و ارتفاع الناشر.

الكلمات المفتاحية: الحمل الحراري الطبيعي، المدخنة الشمسية، تقريب بوسينيسك، المحاكاة العددية.

Résumé

Cette étude se concentre sur une analyse numérique bidimensionnelle de l'écoulement laminaire résultant de la convection naturelle au sein d'une cheminée solaire. Le modèle mathématique repose sur les équations de continuité, de quantité de mouvement et d'énergie formulées dans un système de coordonnées cylindriques, en intégrant l'approximation de Boussinesq. La simulation a été réalisée à l'aide du logiciel COMSOL Multiphysics. Nos résultats ont révélé une forte corrélation entre les performances de la cheminée solaire et la hauteur du diffuseur.

Mots clés : Convection naturelle, cheminée solaire, approximation de Boussinesq, simulation numérique.